Sedimentary Geology 291 (2013) 62–83

Contents lists available at SciVerse ScienceDirect

Sedimentary Geology

journal homepage: www.elsevier.com/locate/sedgeo

Late Miocene to Plio-Pleistocene fluvio-lacustrine system in the Karacasu Basin (SW Anatolia, Turkey): Depositional, paleogeographic and paleoclimatic implications

Hülya Alçiçek [a,*], Gonzalo Jiménez-Moreno [b]

[a] Department of Geological Engineering, Pamukkale University, TR-20070 Denizli, Turkey
[b] Departamento de Estratigrafía y Palaeontología, Universidad de Granada, Fuente Nueva S/N, 18002, Granada, Spain

ARTICLE INFO

Article history:
Received 1 February 2012
Received in revised form 12 March 2013
Accepted 17 March 2013
Available online 6 April 2013

Editor: B. Jones

Keywords:
Continental basins
Pollen
Stable isotopes
Paleoclimate
Neogene
Western Anatolia

ABSTRACT

The sedimentary record of the late Cenozoic Karacasu Basin, a long-lived continental half-graben from southwestern Turkey, is characterized by siliciclastic and carbonate deposits. Sedimentation was controlled by an active NW–SE trending major normal fault along the basin's southern margin and by climatically-induced lake-level changes. Detailed facies analysis subdivides the entire Neogene–Quaternary basin-fill into three distinct litostratigraphic units representing paleogeographic changes and sedimentation patterns throughout the basin evolution.

Sedimentation commenced in the late Miocene with the deposition of proximal–medial alluvial fan and fluvial facies (Damdere Formation; FA1). At this stage, alluvial fans developed in elevated areas to the south, prograding towards the basin center. At the beginning of the Pliocene, fresh to slightly alkaline, shallow lake deposits (FA2a) of the Karacaören Formation formed. The lake became open and meromictic conditions developed (FA2b). Pollen data from the FA2b facies show that climate was arid to humid. Climate probably changed cyclically through time producing alternation of *Artemisia* steppe (cold and dry periods) and more forested vegetation (warm and wet). The open lake facies passes upwards into lake margin facies (FA2c), but it was still dominated by alkaline to slightly saline lake conditions. Sedimentation was almost continuous from the late Miocene to Pleistocene.

In the early Quaternary, the basin was dissected by the re-activation of basin bounding faults. The unconformable base of the overlying Quaternary deposits (Karacasu Formation; FA3) reflected the basin's transformation from a half-graben into a full-graben system. Oxygen isotope data from carbonates show an alternation of humid climatic periods, when freshwater settings predominated, and semiarid/arid periods in which the basin hosted alkaline and saline water lakes. Neotectonic activity has rejuvenated many of the basin-bounding faults, causing development of talus aprons and local alluvial fans. The basin was progressively incised by modern rivers that have largely smoothed out the topographic relief of the graben margins.

© 2013 Elsevier B.V. All rights reserved.

1. Introduction

Western Anatolia contains one of the best examples of intracontinental tectonics. Widespread Neogene and Quaternary crustal extension formed a complex mosaic of NW–SE, NE–SW, and E–W trending basins hosted by the Paleozoic–Mesozoic metamorphic bedrock of the Menderes Massif and the Mesozoic Lycian allochthonous units (e.g., Pamir and Erentöz, 1974; Okay, 1989; Sun, 1990; Bozkurt, 2001). These extensional intramontane basins were filled by Cenozoic siliciclastic to carbonate deposits, such as in the Karacasu Basin. This basin is a NW–SE trending, arcuate half-graben that is approximately 18 km wide and 35 km long (Fig. 1) with Neogene to Quaternary fill which is the subject of this study.

The Neogene and Quaternary were marked by paleogeographic and paleoclimatic changes in the circum-Mediterranean area. The western Anatolian intramontane basins and their sedimentary basin-fill successions are well-exposed with little deformation and commonly contain abundant fossil fauna and flora remains that provide a regional interbasinal geochronologic correlation. There is a significant number of studies devoted to geodynamic setting and tectonic development of the area (Şengör, 1987; Bozkurt, 2001; Ring et al., 2003; Ten Veen et al., 2009; Alçiçek and Ten Veen, 2008; van Hinsbergen, 2010; van Hinsbergen and Schmid, 2012; and references therein), but studies regarding paleoenvironmental and paleoclimatic reconstructions of ancient lakes by means of sedimentologic, mineralogic, and stable isotope geochemistry techniques are rare (Alçiçek et al., 2005; Alçiçek, 2007; Alçiçek et al., 2007; Alçiçek, 2009, 2010).

Previous geologic studies on the Karacasu Basin have primarily focused on its stratigraphy, geothermal potential, and sulfur occurrences (e.g., Nebert, 1955; Becker-Platen, 1970; Kastelli, 1971; Roberts, 1988; Açıkalın, 2005; Alçiçek and Mayda, 2009; and references therein). Comprehensive geologic mapping of the region and a lithostratigraphic division of the basin-fill were published by Nebert (1955) and Becker-Platen (1970), with a more recent refinement by Açıkalın (2005) and Konak and Şenel (2002).

* Corresponding author. Tel.: +90 258 2963396; fax: +90 258 2963382.
E-mail address: halcicek@pau.edu.tr (H. Alçiçek).

0037-0738/$ – see front matter © 2013 Elsevier B.V. All rights reserved.
http://dx.doi.org/10.1016/j.sedgeo.2013.03.014

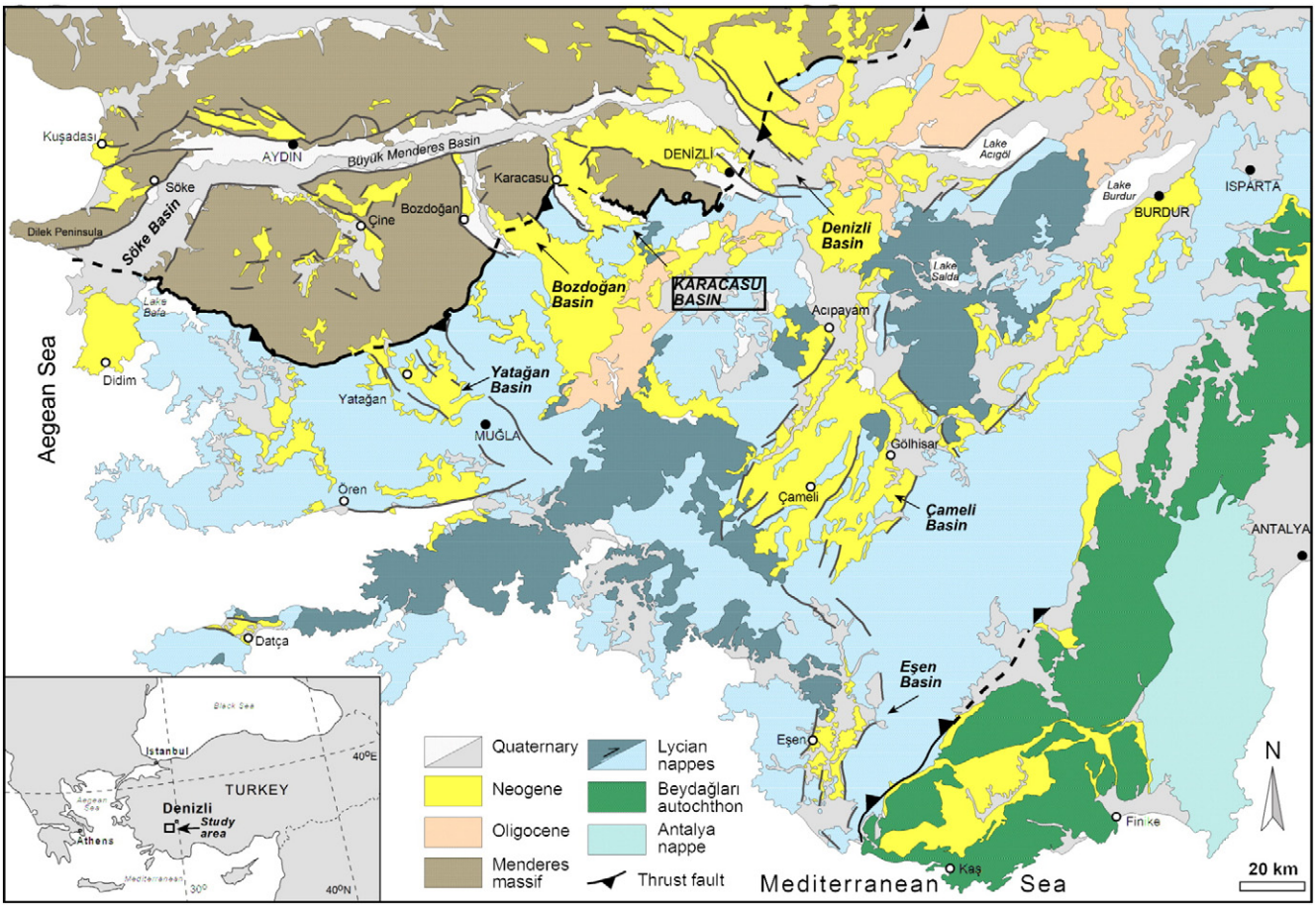

Fig. 1. Overview of the prominent extensional basins of western Anatolia surrounding the Karacasu Basin (Konak and Şenel, 2002).

This study deals with the analysis of depositional, paleoenvironmental and paleohydrological evolution of the lacustrine system(s) developed in the Karacasu Basin by using sedimentologic, mineralogic, geochemical and palynologic analyses. One of the aims is to establish the response of this system to the short- and long-term tectonic, geomorphologic, and climatic changes that affected the basin's catchment system. The lacustrine archives of this basin will add to the synthesis of regional data with paleogeographic, paleoclimatic, biogeographic, and paleoecologic information and will contribute to regional Neogene paleogeography and paleoclimatology in the eastern Mediterranean.

2. Geologic setting and basin stratigraphy

The pre-Oligocene bedrock in southwestern Anatolia (Fig. 1) consists of: (1) the metamorphic Menderes Massif; (2) the Beydağları crustal block with an unknown basement overlain by a thick platform of Mesozoic carbonates; (3) the Lycian nappes composed mainly of Mesozoic cherty carbonates and late Mesozoic–Paleogene ultramafic rocks; and (4) the Antalya nappes dominated by ophiolites. These bedrock units represent the closure of the Neotethyan oceanic basin during the Mesozoic–early Cenozoic that involved the genesis and emplacement of large-scale carbonate platforms and ophiolitic units (Collins and Robertson, 1997, 1998).

The Karacasu Basin rests on metamorphic rocks of the Menderes Massif and ophiolitic and carbonate rocks of the Lycian nappes. The southern margin of the Karacasu Basin is defined by a prominent, NE-dipping normal fault separating the basin fill deposits from bedrock (Fig. 2). The fault-bounded SW margin of the basin corresponds to the escarpment of the Karıncalıdağ Mountain range (altitude ~1699 m), whereas the NE margin has a more subdued topography bounded by a plateau with an altitude of ~850 m. The basin interior is characterized by a series of NW–SE trending normal faults that accentuate the half-graben structural configuration, with a mean elevation of the basin-floor at ~150 m.

The Neogene to Quaternary basin-fill succession of the Karacasu Basin, up to 430 m thick, consists of siliciclastic alluvial deposits and lacustrine lutites and carbonates, which are best exposed along the basin margins. The lithostratigraphy of the basin-fill succession was studied by Nebert (1955), Becker-Platen (1970), and Roberts (1988). More recently, Açıkalın (2005) designated the main late Miocene–Pliocene part of the basin-fill succession as the Dandalas Group and divided it into the Damdere Formation (late Miocene) and the Karacaören Formation (Pliocene). The Dandalas Group is the stratigraphical equivalent of the fluvio-lacustrine series in the neighboring basin of the Bozdoğan (Fig. 1) to the west in which a Pikermian fauna (MN11–13 biozone, late Tortonian–Messinian) was determined by Roberts (1988). They are overlain by relatively thin Pleistocene deposits [MN17-Gelasian-biozone by Açıkalın (2005)] of the Karacasu Formation and are covered unconformably by younger Quaternary alluvium deposits (see Figs. 2 and 3). The stratigraphic correlation of the Karacasu Basin to the neighboring basins was done by Alçiçek (2010).

2.1. The Damdere Formation

This unit forms the lower part of the basin-fill succession and overlies the bedrock unconformably, passing upwards into the Karacaören Formation (Becker-Platen, 1970; Açıkalın, 2005; Fig. 2). Sedimentation was controlled by the basin's southern boundary

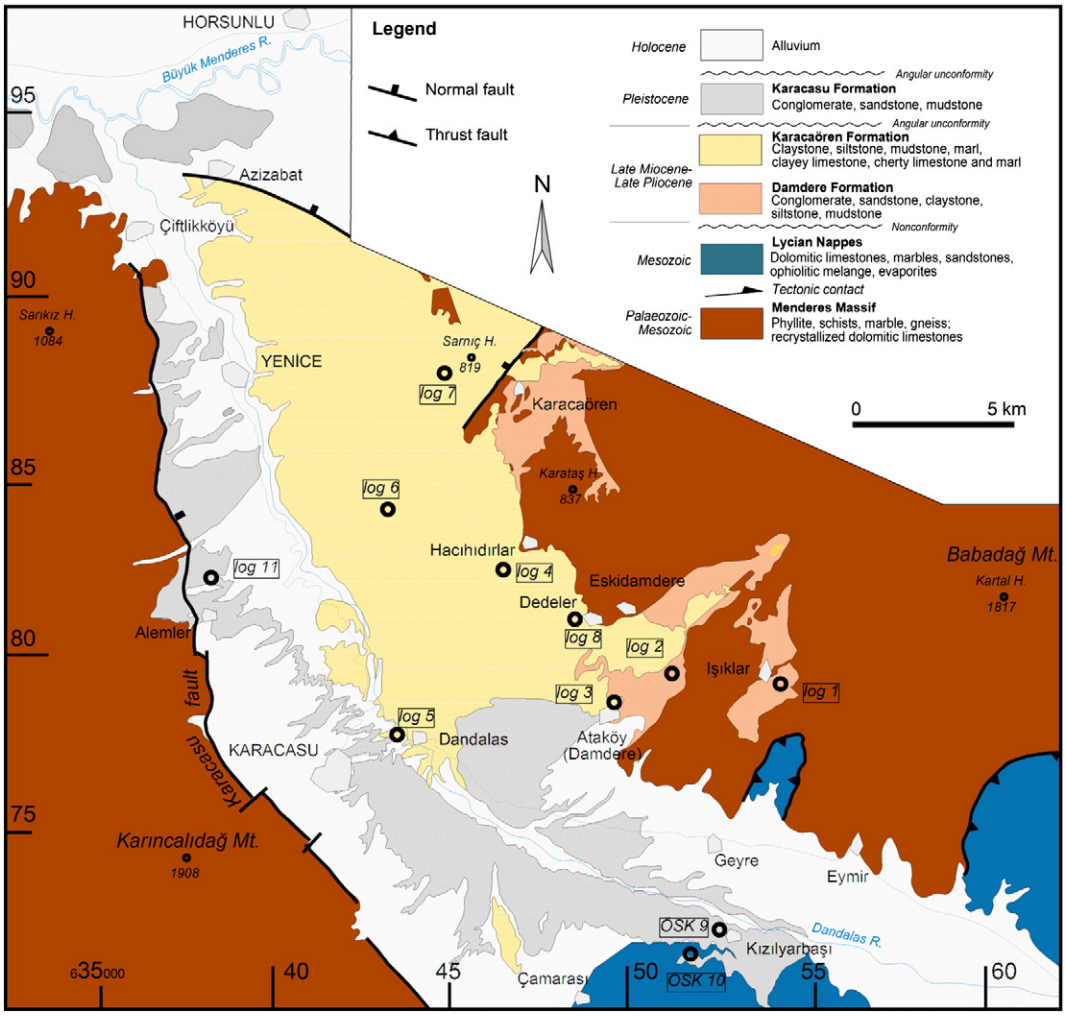

Fig. 2. Geologic map of the Karacasu Basin (the locations of the measured sections are indicated). The map is based on Konak and Göktaş (2002) and the geological map sheet series of the Mineral Research and Exploration Directorate of Turkey by the courtesy of N. Konak, pers. commun., 2010.

fault. The unit is up to 150 m thick and is composed of two subunits: (1) a lower unit of matrix-supported coarse-grained conglomerates alternating with reddish mudstones; and (2) an upper unit of yellowish-red, clast-supported channelized conglomerates. The multistory paleochannels, in many cases, grade upwards into fine-grained sandstones, siltstones, and reddish massive and organic-rich mudstone deposits.

2.2. The Karacaören Formation

This formation is up to 210 m thick and is divided into two subunits: (1) a lower unit of alternating sandstone, marlstone, mudstone, and clayey limestone, and dolomite, ca. 100 m thick; (2) an upper unit of alternating bituminuous shale, marlstone and bioclastic dolomite, ca. 55 m thick; and overlain by alternating sandstone, marlstone, diatomite, cherty marlstone and limestone, and clayey limestone and dolomite, ca. 55 m thick.

2.3. The Karacasu Formation

The uppermost formation rests uncomformably on the underlying formations in the southern part of the basin and overlies unconformably the metamorphic bedrock in the northern part of the basin (Becker-Platen, 1970; Açıkalın, 2005). This formation is up to 70 m thick and consists of two subunits: (1) a lower unit of matrix-supported coarse-grained conglomerates alternating with reddish laminated siltstone–mudstone and massive mudstones, ca. 50 m thick; and (2) an upper unit of weakly cemented, yellowish- to brownish-gray conglomerates, sandstones, and mudstones with sulfur-bearing nodules, ca. 20 m thick with vertebrate remains, including equids and bovids [biozone MN17, late Villanyian; Karacasu locality; Açıkalın (2005)].

The youngest deposits of the basin show an unconformable, erosional base and include the fluvial deposits of modern rivers, local basin-margin alluvial fans, extensive colluvial (talus) aprons, and modern soil cover (Fig. 3).

3. Material and methods

The basin-fill succession has been studied by detailed sedimentologic logging of eleven outcrop sections. Macroscopic facies analysis was supplemented by observation of thin sections of the collected samples. The studied deposits were divided into twenty-six sedimentary facies, which have been further grouped into three facies associations (Table 1). The descriptive terminologies of Miall (1996) and Arenas and Pardo (1999) have been followed.

The mineralogic composition of 73 powdered carbonate samples was determined by X-ray diffraction (XRD). X-ray identification and clay fractionation was performed at TPAO Research Centre Laboratories (Turkish Petroleum Corporation, Ankara, Turkey). Powder X-ray diffraction patterns of the samples were recorded on a Rigaku D/Max 2200 PC diffractometer using CuKa radiation (k = 1.542 Å). The semi-quantitative

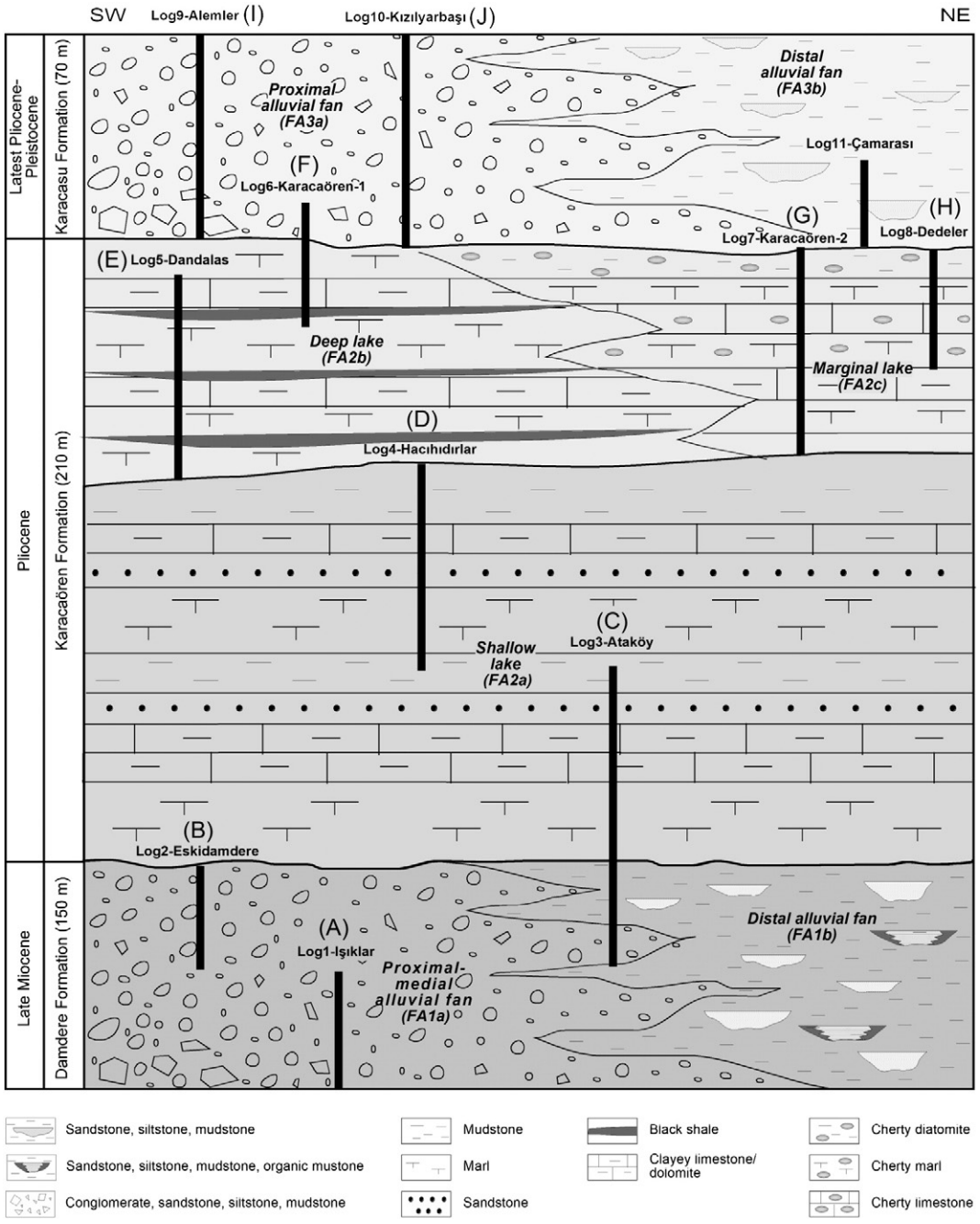

Fig. 3. Stratigraphy of the basin-fill succession of the Karacasu Basin showing sedimentary logs (see Fig. 2 for location of the sections) with the sampling levels (see Fig. 4A–K) (not to scale). Based on Açıkalın (2005) and Alçiçek and Mayda (2009).

ratios were determined from the powder diffractogram following an external standard method developed by Temel and Gündoğdu (1996).

Values of mol% $CaCO_3$ of the carbonate minerals were estimated by measurement of the position of d_{104} peak relative to a standard (Goldsmith et al., 1961). The degree of ordering of the dolomite crystals was determined by the sharpness and relative intensities of the ordering peaks, with superstructure reflections corresponding to d_{21}, d_{015} and d_{110} (Goldsmith and Graf, 1958). The degree of ordering is thus estimated by the ratio of the heights of the ordering peak 015 to the diffraction peak 110 (Hardy and Tucker, 1988).

Stable isotope samples were collected by drilling micritic carbonate textures and obtaining 0.5–3 mg of powdered sediment. Samples with diagenetic alteration were eliminated and only dense micritic areas were drilled for isotopic analysis. Stable isotope analyses were performed on these carbonate samples ($\delta^{18}O$ and $\delta^{13}C$ data, see Table 2). The $\delta^{18}O$ and $\delta^{13}C$ analyses were carried out at the Iso-Analytical Laboratory in Cheshire, U.K., according to the method of Coplen et al. (1983). For mixed carbonate samples, both calcite and dolomite were analyzed if the lesser mineral constituted at least 10% of the total carbonate. Otherwise, only the dominant mineral was analyzed. Carbon dioxide was evolved from each sample at 25 °C using 100% H_3PO_4. The gas evolved in the first hour was analyzed as calcite; the gas evolved between 24 h and 7 days was analyzed as dolomite. The NBS-19 and NBS-18 standards were used for calibration and correction. These analyses were reported with respect to the PDB standard.

Stable organic carbon isotope ratios were analyzed on black shale samples using EA-IRMS (Elemental Analyzer Isotope Ratio Mass Spectrometry) at Iso-Analytical Laboratories (Cheshire, UK). Carbon dioxide peaks were separated by a packed column gas chromatograph, held at an isothermal temperature of 110 °C, and were entered as

Table 1
Sedimentary facies, facies associations and subassociations distinguished in the Neogene succession of the Karacasu Basin.

Facies	Description	Interpretation
Gm Matrix-supported conglomerate	Granule to boulder-grade clasts, mud or sand matrix, reddish-brown, poorly sorted to unsorted, subangular to subrounded, up to 2.5 m thick beds, ungraded to poor inversely graded, common erosional boundaries, lenticular bodies with up to 1.5 m thick and 3–4 m wide, intercalated with facies Gc	Subaerial plastic debris flows
Gc Clast-supported conglomerate	Granule to boulder-grade clasts, moderately- to poorly-sorted, muddy sand matrix, reddish-brown, subangular to subrounded, 50 cm to 1 m thick beds, erosional boundaries, lenticular bodies with up to 2 m thick and up to 15 m wide, intercalated with facies Gm	Subaerial hyperconcentrated flow deposits in channels
Gh Horizontally stratified conglomerates	Granule to pebble-grade clasts, poorly- to moderately-sorted, sand, silt, and mud matrix, reddish-brown, subangular to subrounded, 50–100 cm thick beds, horizontal to gently inclined (<15°), ungraded, poorly imbricated, slightly erosional to non-erosional bases, a few tens of meters in lateral extent, intercalated with facies Gp and Sm	Episodic, sediment charged flash floods
Gp Planar cross-stratified conglomerate	Pebble- to cobble-grade clasts, reddish brown, poorly sorted mixture of sand and mud matrix, subangular to subrounded, forming beds up to 30 cm thick, solitary cross-sets, 50–150 cm thick sets, lenticular geometry, erosional and concave-upward bases, alternating with facies Gh and Sm	Powerful, hyperconcentrated floods
Sm Massive (pebbly) sandstone	Fine- to coarse-grained sandstone, reddish to dark yellowish-gray, poorly to moderately sorted, unstratified, 5–60 cm thick beds, little or no grain-size graded, several tens of meters in lateral extent, sharp and slightly erosional boundaries, intercalated with facies Gh and Gp	Sediment gravity flows
Fm Massive mudstone	Massive, silty to sandy, dark yellow-red mudstone, forming beds up to 2 m thick, bearing plant remains, elongated casts of micrite (<0.5 cm to >3 cm in length), calcrete nodules, a few tens of meters in lateral extent, intercalated with facies Sm and Fl	Rapid waning of flash flood events
Fl Laminated silty mudstone	Mudstone with thin siltstone layers, thinly parallel laminated, dark yellow-red, bed thickness up to 1.5 m, containing plant detritus, ostracodes and gastropods, a few tens of meters in lateral extent, alternating with facies Sm1, Fm, and C	Suspension settling dominantly from standing water
C Organic mudstone	Dark gray to black laminated mudrocks, containing plant remains and elongated casts of micrite (<0.7 cm to >4 cm in length), up to 30 cm thick beds, a few ten of meters in lateral extent, intercalated with facies Sm and Fl	Vegetated swamp and marsh areas
Sm1 Massive (pebbly) sandstone	Fine- to medium-grained pebbly sandstone, beige to yellow, moderately to well sorted, non-stratified, 30–150 cm thick beds, tens of meters in lateral extent, intercalated with facies Fl1 and Fl3	Transitional siliciclastic/carbonate mudflat to a limy marsh to shallow lake
Fl1 Laminated marlstone	Parallel laminated light-green to gray marlstones, 20 cm to 100 cm thick beds, including mud cracks, plant detritus and elongated casts of micrite (<1 cm to >10 cm in length), several tens of meters in lateral extent, intercalated with Sm1, Lm1, Lm2 and Fl3	Carbonate and siliciclastic sedimentation in littoral to shallow lacustrine zones
Fl2 Clayey marlstone	Parallel-laminated, locally massive clayey marlstones, dark greenish-gray, forming beds 2–50 cm thick, several tens of meters in lateral extent, containing mudcracks, plant detritus and elongated casts of micrite (from less than 1 cm to several centimeters long), alternated with facies Fl1, Fl3, Lm1 and Lm2	
Fl3 Massive mudstone	Massive mudstones, beige to yellow, commonly silty or sandy, forming tabular beds 20–100 cm thick, several tens of meters in lateral extent, containing thin marlstone and siltstone intercalations (0.5 cm in thickness), plant detritus, and mudcracks, intercalated with facies Fl1, Fl2, Lm1 and Lm2	Low-energy proximal lacustrine settings
Fl4 Black shale	Dark gray to black, claystone with thin bituminous laminae (1–5 mm thick), 30 cm to 150 cm thick beds, containing native sulfur nodules (5–25 cm thick), ostracodes, lenticular gypsum crystals (3–7 mm in size), diatoms, algae, and pollen, several tens of meters in lateral extent, alternating with facies Lm3 and Fl5	Anoxic, stratified deep lake, with a high bioproductivity
Fl5 Gray marlstone	Gray marlstones, dark gray to brown, form tabular to slightly lenticular beds, 30 cm to 200 cm thick, several tens of meters in lateral extent, parallel-laminated, rarely massive, contains ostracode, mollusc, and organic matter, alternated with facies Fl4 and Lm3	Suspension settling in deep lacustrine zones
Fl6 Cherty marlstones	White to beige, parallel-laminated or massive marlstones, tabular to slightly lenticular beds (20 cm to 150 cm thick), containing chert nodules and diatoms, several tens of meters in lateral extent, intercalated with Fl1, Fl2, and Lm4	Mixed carbonate and fine-grained siliciclastic deposition in marginal lake environment
Fl7 Cherty diatomite	Beige to brown, parallel-laminated (0.3–0.9 cm in thickness), rarely massive diatomites, tabular to slightly lenticular beds (30 cm to 150 cm thick), containing chert nodules, several tens of meters in lateral extent	The deposition of silica by diatoms in shallow lake
Lm1 Clayey limestone	Beige to yellow grainstones and mudstones to packstones, tabular beds (20–100 cm thick), comprising lenticular rosette-like gypsum pseudomorphs and rarely ostracodes, molluscs and charaphytes, several tens of meters in lateral extent, intercalated with facies Fl1, Fl2, Fl3, and Lm2	Carbonate precipitation in shallow lake, freshwater limestones

Table 1 (*continued*)

Facies	Description	Interpretation
Lm2 Clayey dolomite	Beige to yellow mudstones to wackestones, tabular beds 30–150 cm thick, containing displacive lenticular to prismatic gypsum crystals (0.2 mm to 2 cm in size), circumgranular and planar cracks, plant remains, elongated casts of micrite (<0.5 cm to >4 cm in length), charophytes and small cavities (up to 1 mm), several tens of meters in lateral extent, intercalated with facies Lm1, Fl1, Fl2, and Fl3	Deposition of Mg-rich carbonate mud in a low-energy palustrine, periodically drying lake-margin environment
Lm3 Bioclastic dolomite	Beige-yellow to light brown wackestones to packstones, massive tabular beds 10–100 cm thick, containing ostracodes, several tens of meters in lateral extent, intercalated with facies Fl4 and Fl5	Deposition of Mg-rich carbonate mud in low-energy, open lake environment
Lm4 Cherty limestone	Beige to yellow mudstones to wackestones with homogeneous micritic matrix, diffuse rare ostracodes, circumgranular and planar cracks and small cativies, forming tabular beds 30–150 cm thick, several tens of meters in lateral extent, intercalated with facies Fl1, Fl2, and Fl6	Sublittoral zone in shallow alkaline carbonate lake

the ion source of Europa Scientific GEO 20-20 IRMS to be ionized and accelerated. Gas species of different masses were separated in a magnetic field and simultaneously collected using a Faraday cup collector array to measure the isotopomers of CO_2 at m/z 44, 45, and 46. The reference material used for the analyses was the IA-R002 oil standard with a $\delta^{13}C$ value of −28.06‰ vs. V-PDB of Iso-Analytical Lab.

Ten carbonate and chert samples were studied using a ZEISS EVO 50 scanning electron microscope (SEM) equipped with an Oxford Instruments INCA EDX unit (Hacettepe University, Ankara, Turkey).

Eleven black shale samples were processed for Rock-Eval pyrolysis and were analyzed at TPAO (Turkish Petroleum Corp.) Research Center Organic Geochemistry Laboratories for total organic carbon (TOC). Rock-Eval pyrolysis was performed on 100 mg crushed rock samples. Samples were heated to 600 °C in a helium atmosphere, using a TOC module equipped a Rock-Eval 6 (RE-6) type instrument.

Five samples have been studied for pollen analysis. These come from bituminous shales and marlstones from the Karacaören Formation. Many other samples from other sections (Ataköy and Dedeler sections) were processed for pollen but samples were barren. Sample processing included digestion by acids (HCl and HF), heavy liquid separation ($ZnCl_2$; density = 2) and sieving (10 μm). The pollen residue, mounted in glycerine, was prepared on slides. Pollen identification and counting was carried out with a transmitted light microscope at ×400 and ×1000 magnifications. A minimum of 150 pollen grains (excluding *Pinus* and indeterminable Pinaceae) was counted in each sample (Cour, 1974). The percentages of pollen taxa were calculated, and the results were plotted in a detailed pollen diagram.

4. Sedimentary facies and depositional systems

Three facies associations are recognized in the Karacasu basin-fill succession and are subdivided on the basis of systematic differences in their grain size, sedimentary structures, textures, fabrics, characteristic styles of stratification, diagenetic overprints, and mineralogy.

4.1. Facies association I (FA1)

This facies association characterizes the Damdere Formation, which is well exposed between the villages of Damdere and Karacaören (Fig. 2). Two main facies subassociations (FA1a and FA1b) are distinguished in this formation (Fig. 3 and section Işıklar in Fig. 4A, Eskidamdere in Fig. 4B, Ataköy in Fig. 4C, and Dedeler in Fig. 4H).

4.1.1. Subassociation FA1a

These deposits occur in the lower part of the Damdere Formation, cropping out at the southwestern fringe of the basin (see the Işıklar section in Fig. 4A, Eskidamdere section in Fig. 4B, and Ataköy in Fig. 4C), and are composed of an up to 90 m thick succession of reddish-brown siliciclastic rocks. The thickness of this facies assemblage increases towards the basin-margin fault (Karacasu fault; see Fig. 2), and the basinward lateral extent is relatively short, on the order of several tens of meters, where the deposits of FA1a interfinger with those of FA1b (Fig. 4). The deposits of FA1a have been subdivided into two lithofacies, FA1a.1 and FA1a.2:

FA1a.1 deposits comprise disorganized, clast-supported, boulder to cobble conglomerate (facies Gc) and matrix-supported conglomerate (facies Gm). The typical characteristics of FA1a.1 include poorly sorted, angular to subrounded clasts, a(t)b(i) imbrication, wide range of particle sizes (very coarse sand to cobble), crude fining upward, and lenticular geometries of individual units. Facies Gm occurs in lenticular units that are up to 1.5 m thick and 3–4 m wide. This facies is poorly sorted to unsorted and includes clasts ranging in size from granule to boulder (Fig. 5A). Facies Gc consists of reddish-brown, nonstratified, granule to boulder-grade conglomerates (Fig. 5B). Beds are 50 cm to 1 m thick with erosional boundaries. This facies occurs within lenticular units that are approximately 2 m thick and up to 15 m wide.

FA.1a.2 deposits consist of normally graded, clast-supported conglomerates (facies Gh and Gp) interbedded with lenses of massive sandstones (facies Sm). Individual gravel bodies are up to 2 m thick and several tens of meters wide. Multistory beds with internal erosional surfaces are thick and common. Facies Gh are composed of horizontal to gently inclined (<15°), ungraded, granule- to pebble-grade conglomerates. Beds are 50–100 cm thick with slightly erosional to non-erosional bases. Facies Gp consists of reddish brown, pebble- to cobble-grade conglomerates with clast-supported texture and planar cross-stratification (Fig. 10C). Cross-strata sets are mainly up to 30 cm thick, forming cosets 50–150 cm in thickness, with lenticular geometry and erosional, concave-upward bases. Facies Sm consists of reddish to dark yellowish-gray, fine- to coarse-grained, massive sandstones, poorly to moderately sorted (Fig. 5C). Beds are 5–60 cm thick, mainly tabular, and several tens of meters in lateral extent, with sharp, slightly erosional bases and little or no grading.

4.1.1.1. Interpretation. Texturally immature, coarse conglomerates of FA1a.1 occur in the proximal areas of the fan, close to the southwestern boundary fault of the basin. The clast-supported framework, lack of inverse grading, a(t)b(i) imbrication, an erosional lower boundary and crude stratification of the disorganized conglomerates of FA1a.1 (facies Gc and Gm) indicate a streamflow origin (Ridgway and DeCelles, 1993; Hadlari et al., 2006).

The presence of the multistory, superposed distinct conglomeratic facies of FA1a.2 implies an episodic, unconfined, sediment-charged flash floods in the middle part of the alluvial fan (Abdul Aziz et al., 2003; Capuzzo and Wetzel, 2004). The sheet-like geometry and the

Table 2
Oxygen and carbon isotope values of Neogene carbonate deposits from the Karacasu Basin (m = mudstone, w = wackestone).

Formation/facies assoc.	Facies-faciess code/microfacies	Sample no/section	Calcite		Dolomite	
			$\delta^{13}C$	$\delta^{18}O$	$\delta^{13}C$	$\delta^{18}O$
Karacasu Formation FA3b: Distal alluvial fan	Calcrete-Fm (m)	KB.3 (Kızılyarbaşı)	−9.40	−5.87		
	Calcrete-Fm (m)	KB.1	−9.37	−5.95		
	Calcrete-Fm (w)	CM.9 (Çamarası)	−8.18	−7.01		
	Calcrete-Fm (m)	CM.7	−7.26	−7.46		
	Calcrete-Fm (w)	CM.6	−7.26	−6.33		
	Calcrete-Fm (m)	CM.5	−7.21	−7.77		
	Calcrete-Fm (m)	CM.3	−5.17	−7.10		
	Calcrete-Fm (w)	CM.1	−11.01	−5.60		
Karacaören Formation FA2c: Marginal lake	Clayey limestone-Lm1 (m)	KR.18 (Karacaören-2)	−1.98	0.97	−2.17	1.58
	Marlstone-Fl2 (m)	KR.17			−0.54	−0.07
	Marlstone-Fl1 (m)	KR.16	−1.21	0.65	−0.87	−0.08
	Marlstone-Fl1 (m)	KR.15			−0.25	−3.35
	Marlstone-Fl2 (m)	KR.14	−0.41	0.54	−2.81	−0.20
	Clayey dolomite-Lm2 (w)	KR.10			−1.29	−2.94
	Marlstone-Fl1 (m)	KR.7			−2.59	−0.33
	Marlstone-Fl2 (m)	KR.5			−0.08	1.05
	Clayey limestone-Lm1 (m)	KR.4	−0.20	−0.63		
	Clayey dolomite-Lm2 (w)	KR.3	1.11	2.53	0.89	2.31
	Marlstone-Fl1 (m)	KR.2			2.98	3.82
	Clayey dolomite-Lm2 (m)	KR.1			1.37	0.93
Karacaören Formation FA2b: Open lake	Marlstone-Fl5 (m)	KRC.7 (Karacaören-1)	0.96	−5.30	−1.23	−2.74
	Marlstone-Fl5 (m)	KRC.5	1.37	−6.32	1.18	−5.83
	Clayey dolomite-Lm2 (w)	KRC.4	0.69	−8.34	0.63	−7.95
	Marlstone-Fl5 (m)	KRC.2	1.33	−8.79	0.92	−8.47
	Marlstone-Fl5 (m)	KRC.1	1.21	−8.65		
	Marlstone-Fl5 (m)	DAN.5 (Dandalas)	−0.99	2.67		
	Marlstone-Fl5 (m)	DAN.4	−1.65	1.13		
	Marlstone-Fl5 (m)	DAN.3	−2.35	3.76	−1.74	4.71
	Marlstone-Fl5 (m)	DAN.2	−2.21	4.04	−1.60	4.82
	Marlstone-Fl5 (m)	DAN.1	−4.26	5.89	−1.35	5.04
Karacaören Formation FA2a: Shallow lake	Clayey dolomite-Lm2 (m)	HH.57 (Hacıhıdırlar)			3.30	−1.14
	Clayey dolomite-Lm2 (m)	HH.52			7.10	0.27
	Clayey dolomite-Lm2 (w)	HH.40			2.12	−0.44
	Clayey dolomite-Lm2 (w)	HH.36			−2.28	−3.67
	Clayey dolomite-Lm2 (m)	HH.32			1.40	−3.50
	Clayey dolomite-Lm2 (w)	HH.30			−2.73	−2.33
	Marlstone-Fl1 (m)	HH.29			−4.54	−3.51
	Clayey dolomite-Lm2 (m)	HH.28			−2.15	−1.24
	Clayey dolomite-Lm2 (w)	HH.26			−2.52	−0.85
	Clayey dolomite-Lm2 (m)	HH.24			−4.11	0.96
	Marlstone-Fl1 (m)	HH.22			−2.81	1.18
	Marlstone-Fl2 (m)	HH.19			−5.44	−5.30
	Clayey dolomite-Lm2 (w)	HH.16			−5.27	−0.20
	Marlstone-Fl2 (m)	HH.8			−4.95	−2.15
	Clayey dolomite-Lm2 (w)	HH.6			−4.95	−2.71
	Clayey dolomite-Lm2 (m)	HH.5			−5.25	0.38
	Mudstone-Fl3 (m)	HH.4			−5.00	−1.45
	Clayey dolomite-Lm2 (w)	HH.2			−2.66	0.00
	Clayey limestone-Lm1 (w)	AT.30 (Ataköy)	−4.79	−6.27		
	Clayey limestone-Lm1 (m)	AT.28	−0.61	−8.50		
	Clayey limestone-Lm1 (m)	AT.27	−3.02	−5.31	−3.36	−3.37
	Clayey limestone-Lm1 (w)	AT.26	−3.48	−5.51	−2.72	−4.98
	Clayey dolomite-Lm2 (w)	AT.25	−1.83	−6.69	−2.42	−5.05
	Clayey dolomite-Lm2 (m)	AT.24			−2.78	2.73
	Marlstone-Fl1 (m)	AT.22			−0.71	−0.64
	Clayey limestone-Lm1 (m)	AT.21	−0.98	−8.75		
	Clayey dolomite-Lm2 (w)	AT.19			1.63	−0.73
	Marlstone-Fl2 (m)	AT.18			−2.13	−1.14
	Marlstone-Fl1 (m)	AT.16			−1.32	1.06
	Clayey dolomite-Lm2 (m)	AT.15			1.57	0.04
	Clayey dolomite-Lm2 (m)	AT.13			2.12	0.34
	Clayey dolomite-Lm2 (w)	AT.10			3.28	2.47
	Clayey dolomite-Lm2 (w)	AT.8	−1.06	−4.19	−0.52	0.77
	Clayey limestone-Lm1 (m)	AT.7	−2.13	−5.59		
	Clayey limestone-Lm1 (w)	AT.5	−1.74	−9.21		
	Marlstone-Fl1 (m)	AT.2			2.57	0.72
	Mudstone-Fl3 (m)	AT.1			1.96	−0.05
Damdere Formation FA1b: Fluvial	Calcrete-Fm (m)	DE.6 (Dedeler)	−6.81	−8.04		
	Calcrete-Fm (m)	DE.5	−6.77	−8.11		
	Calcrete-Fm (w)	DE.4	−6.74	−8.29		
	Calcrete-Fm (m)	DE.3	−6.14	−8.42		
	Calcrete-Fm (w)	DE.2	−6.11	−9.05		
	Calcrete-Fm (m)	DE.1	−5.45	−7.15		

absence of cross-stratification of sandstone facies imply in unconfined interchannel areas by overflows during the high discharge periods (Lee and Chough, 1999).

4.1.2. Subassociation FA1b

This subassociation is well represented in the Ataköy and Dedeler sections (Fig. 4C and H), and is generally well developed in the northern part of the basin. This facies assemblage is up to 60 m thick, and can be followed basinwards over a few kilometers, where it passes laterally into the deposits of FA1a towards the basin margin. They include two main lithofacies, FA1b.1 and FA1b.2:

FA1b.1 deposits consists of laminated silty mudstones (facies Fl), massive mudstones (facies Fm), and organic mudstone beds (facies C). These deposits are up to 30 cm thick laterally persistent beds. This lithofacies has a sheet-like geometry with a lateral extent of several hundred meters and forms 30 m thick intervals. Facies Fm comprises dark yellow to reddish brown, massive mudstones, commonly silty to sandy and bearing plant detritus, elongated casts of micrite (<0.5 cm to >3 cm in length), and carbonate nodules (Fig. 5D). The mudstones are interbedded with 15–50 cm thick massive sandstones (facies Sm). Beds form ribbon-shaped bodies, a few tens of meters in length and <2 m thick, laterally persistent layers. The nodules are composed mainly of hard calcareous concretions of varying sizes and shapes scattered in the host sediment. The nodules are commonly beige and range in size from 10 to 15 cm in diameter (Fig. 5D). They are texturally mudstones to wackestones with a micritic matrix and diffuse circumgranular cracks commonly filled with sparite, plant detritus, and micritic peloids (Fig. 5E). Facies Fl consists of dark yellow to reddish brown, thinly parallel-laminated mudstone with thin siltstone layers (0.5 cm in thickness), containing plant detritus and abundant gastropods and ostracodes (Fig. 5F). Beds are tabular to lenticular, up to 1.5 m thick and a few ten of meters in lateral extent. This facies commonly alternates with organic mudstone (facies C). Facies C is dark gray to black laminated mudrock, containing elongated casts of micrite (<0.7 cm to >4 cm in length), carbonized wood fragments and terrestrial pulmonate gastropods (F. Wesselingh, 2009, pers. comm.). Beds are commonly lenticular, up to 30 cm thick and a few ten of meters in lateral extent (Fig. 5F). Pollen preservation is extremely poor in this facies.

FA1b.2 deposits are represented by about 3 m thick sandstone bodies, which have low width/depth ratio of about 10–15. They are common in mudstones and occur as isolated bodies with convex geometry and steep flanks. The lower boundary is erosional, whereas the upper boundary is erosional or gradational into FA1b.1 deposits. Paleoflow readings show a NE-trend with minor variability.

4.1.2.1. Interpretation. The low width/depth ratio and lenticular geometry of isolated sandstone bodies (FA1b.1) bounded by fine-grained deposits reflect minor lateral channel migration with scouring alternating with bedload transportion and then deposition (Makaske, 2001; Capuzzo and Wetzel, 2004).

The presence of circumgranular fabrics, peloids, etc. in the carbonate nodules formed in the mudstones are evidence of a pedogenic calcretes (Alonso-Zarza, 2003). The surrounding mudstones containing carbonate nodules with small sandstone bodies (FA1b.2) are interpreted as deposits of low-gradient mudflat environments (Abdul Aziz et al., 2003). These mudstones are attributed to bedload transported mud aggregates and settling of suspend sediment from shallow, ponded floodwaters, as suggested by Rust and Nanson (1989) and Gierlowski-Kordesch and Rust (1994).

The organic-rich mudstones developed in lakes or ponds (Makaske, 2001). As reported by Elliott et al. (2007), reducing conditions can exist on inundated floodplain areas in which stagnant water with low dissolved oxygen content increased the preservation of terrestrial organic matter. However, pollen is lacking in these deposits, which could indicate that oxidation was still producing degradation of the pollen grains. Consequently, FA1b deposits imply a rapidly aggrading floodplain environment transecting by low-gradient fluvial channels separated by vegetated areas and wetlands. Therefore, this subassociation is interpreted as an anastomosed river system after Miall (1996).

4.2. Facies association II (FA2)

This association represents the Karacaören Formation, which is well exposed at the northern and southern margins of the basin (Fig. 2) and has been logged at six outcrop sections (see Ataköy in Fig. 4C, Hacıhıdırlar in Fig. 4D, Dandalas in Fig. 4E, Karacaören 1 in Fig. 4F, Karacaören 2 in Fig. 4G, and Dedeler in Fig. 4H). Three facies subassociations have been recognized in this formation:

4.2.1. Subassociation FA2a

These deposits occur in the lower part of the Karacaören Formation and are particularly well-developed in the northeastern part of the basin (Fig. 2). These carbonates and siliciclastics are up to 100 m thick, extend laterally over a few tens of kilometers, and overlie conformably the proximal–medial alluvial fan deposits (FA1b) in the southern part and the distal alluvial fan deposits of FA1b in the northern part of the basin (Fig. 3). The association consists of massive (pebbly) sandstone (facies Sm1), laminated and clayey marlstones (facies Fl1 and Fl2), massive mudstone (facies Fl3), clayey limestone (facies Lm1), and clayey dolostone (facies Lm2) (see the Ataköy section in Fig. 4C and Hacıhıdırlar in Fig. 4D).

Massive (pebbly) sandstone (facies Sm1) is a beige to yellow, pebbly sandstone, fine- to medium-grained and moderately to well sorted, forming beds 30–150 cm thick, a few tens of meters in lateral extent, and alternating with laminated marlstone (Fl1) and massive mudstone (Fl3). This facies is locally disrupted by vertical and horizontal tubes about 2 mm wide and 3 cm long. The tubes are filled by micrite or microspar. The sandstones are massive including micrite as a minor matrix and contain carbonate intraclasts, thin ostracode shells, and elongated casts of micrite (<0.5 cm to >5 cm in length). The laminated marlstone of facies Fl1 is light-green to gray color and forms tabular to slightly lenticular beds that are 20 cm to 100 cm thick and several tens of meters in lateral extent (Fig. 6A). This facies is parallel-laminated, rarely massive, with mudcracks, plant detritus, and elongated casts of micrite (<1 cm to >10 cm in length), and is intercalated with dark yellow-green sandstone (facies Sm1), clayey limestone and dolomite (facies Lm1 and Lm2), and massive mudstone (facies Fl3). The clayey marlstone of facies Fl2 is dark greenish-gray in color and forms tabular or lenticular beds that are 2–50 cm thick. This facies is parallel-laminated, only locally massive, containing mudcracks, elongated casts of micrite (from less than 1 cm to several centimeters long), and plant detritus. Massive mudstone (facies Fl3) is structureless, beige to yellow mudstone, forming tabular beds 20–100 cm thick (Fig. 6B). This facies contains disseminated grains of sand and silt, plant detritus, and mudcracks, and thin marlstone and siltstone intercalations (0.5 cm in thickness).

Clayey limestones (facies Lm1) are beige to yellow, porous, and well-cemented (Fig. 6C). They form massive (non-laminated) tabular beds ca. 20–100 cm thick, and alternate with laminated marlstone (Fl1), clayey marlstone (Fl2), massive mudstone (Fl3), and clayey dolomite (Lm2). They bear lenticular rosette-like gypsum pseudomorphs (Fig. 6D) and ostracodes, molluscs and charophytes (Fig. 6D, E). The rosettes form layers of considerable lateral continuity. They range in size from 0.3 mm to 1.5 cm in diameter. Gastropod shell cavities are open or filled with microsparite (Fig. 6E). Facies Lm1 are texturally

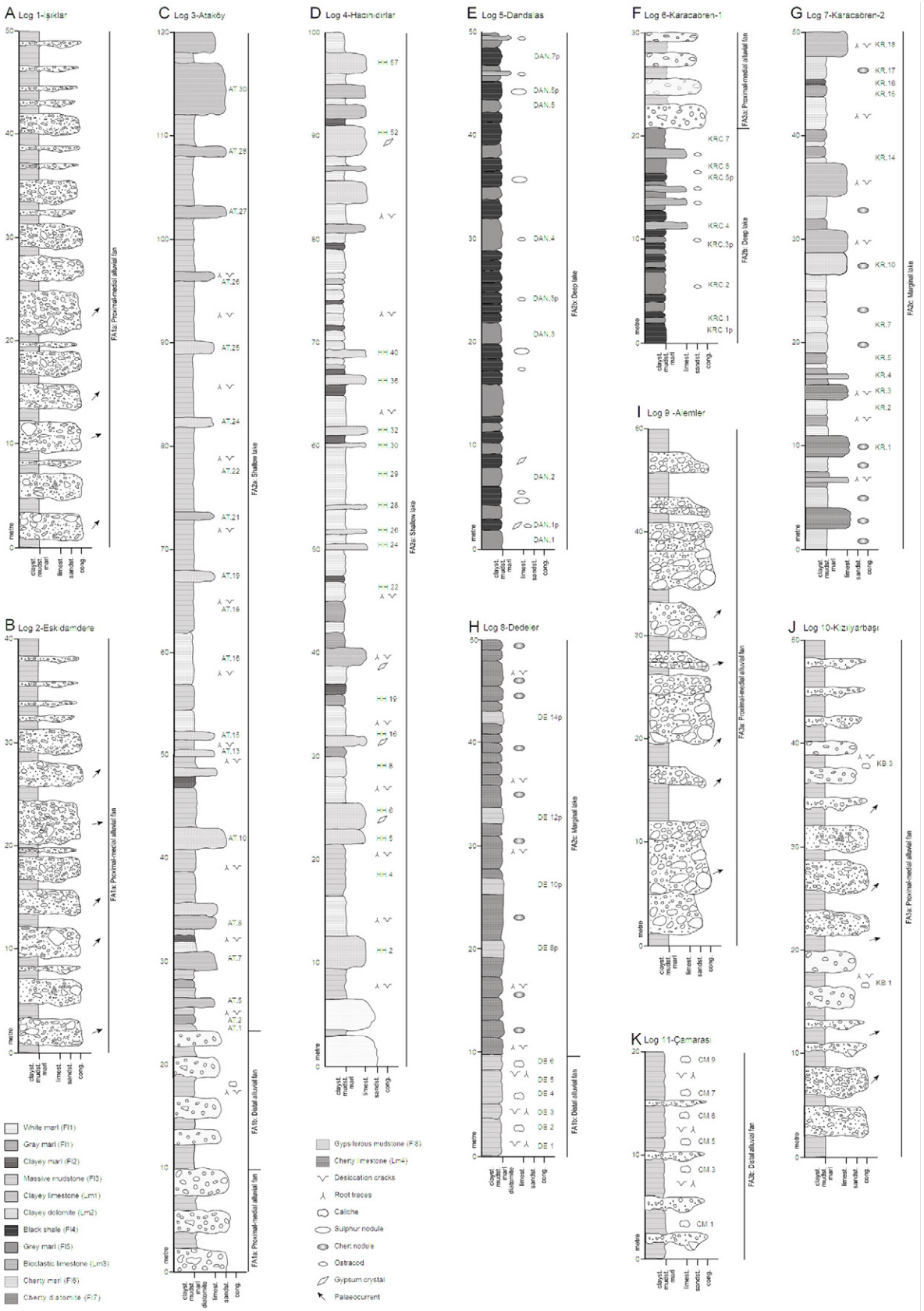

Fig. 4. Measured logs from the Karacasu Basin (see Fig. 2 for outcrop locations); (A, B) The lower and middle part of the Damdere Formation (Işıklar and Eskidamdere sections: logs 1 and 2, respectively); (C) The middle and upper part of the Damdere Formation and lower part of the Karacaören Formation (Ataköy section: log 3); (D) The lower part of the Karacaören Formation (Hacıhıdırlar section: log 4); (E) The middle part of the Karacaören Formation (Dandalas section: log 5); (F) The upper part of the Karacaören Formation and lower and middle part of the Karacasu Formation (Karacaören-1 section: log 6); (G) The upper part of the Karacaören Formation (Karacaören-2 section: log 7); (H) The lower part of the Damdere Formation and upper part of the Karacaören Formation (Dedeler section: log 8); (I, J) The lower and middle part of the Karacasu Formation (Alemler and Kızılyarbaşı sections: log 9 and log 10, respectively); and (K) The upper part of the Karacasu Formation (Çamarası section: log 11).

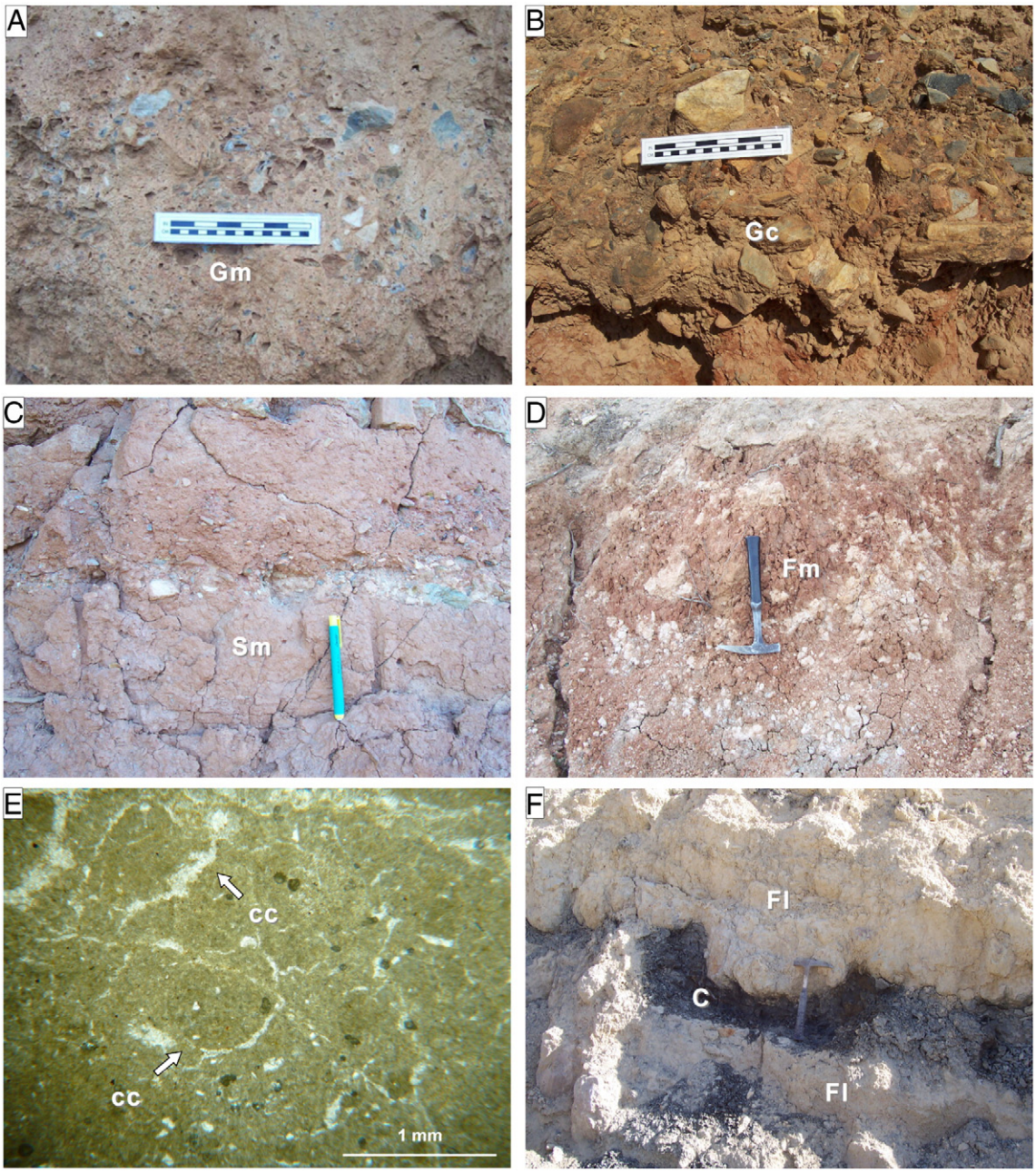

Fig. 5. Facies of the Damdere Formation (FA1; see Fig. 2 for locations); (A) Matrix-supported conglomerate (facies Gm); (B) Clast-supported conglomerate (facies Gc); (C) Massive pebbly sandstone (Sm) (scale: 10 cm); (D) Calcrete nodule-bearing massive mudstone (Fm); (E) Mudstones texture of calcrete nodule with a micritic matrix and diffuse circumgranular cracks (cc); and (F) Alternation of laminated siltstone–mudstone (Fl) and organic mudstone (C).

wackestones to packstones, with a homogeneous micritic matrix, diffuse individual or composite rosette pseudomorphs after gypsum on the mm to cm-scale, planar and circumgranular mudcracks, plant detritus, calcified charophyte stem fragments, and micritic peloids (Fig. 6D–F).

The clayey dolostone of facies Lm2 is beige to yellow in color and forms compact, porous, tabular beds 30–150 cm thick (Fig. 7A), intercalating with clayey limestone (Lm1), laminated and clayey marlstones (facies Fl1 and Fl2) and massive mudstone (facies Fl3). They are texturally mudstones to wackestones composed of homogeneous micritic matrix, with circumgranular and planar cracks, irregular micrite nodules, plant remains, charophytes, and small cavities (Fig. 7B). These cracks are up to 1 mm in size and include planar and circumgranular cracks. Some cracks are completely open, but others are partially filled with micrite, microspar, and/or spar calcite cement (Fig. 6F). Micrite nodules embedded within muddy matrix, or isolated by cracks, are open or filled with sparite cement. The nodules are either vertically or horizontally oriented and are commonly in rounded to angular in shape forming breccias. Peloids are composed of angular or rounded micrite grains (0.5–0.8 mm in diameter). The coated grains consist of irregular and asymmetrical micritic envelopes with nucleus of bioclasts (i.e., ostracodes, charophyte), intraclast fragments, or siliciclastic grains. Displacive lenticular to prismatic gypsum crystals (0.2 mm to 2 cm in size) are scattered through the beds (Fig. 7A).

Dolomite crystals show two different kinds of habits. The first habit of dolomite is rare and consists of a homogeneous idiotopic mosaic composed of subhedral to rhombohedral crystals 4–8 μm in size (Fig. 7C). The second habit is predominant and composed of smaller crystals, mainly between 0.5 and 1.5 μm in size, forming clusters. These

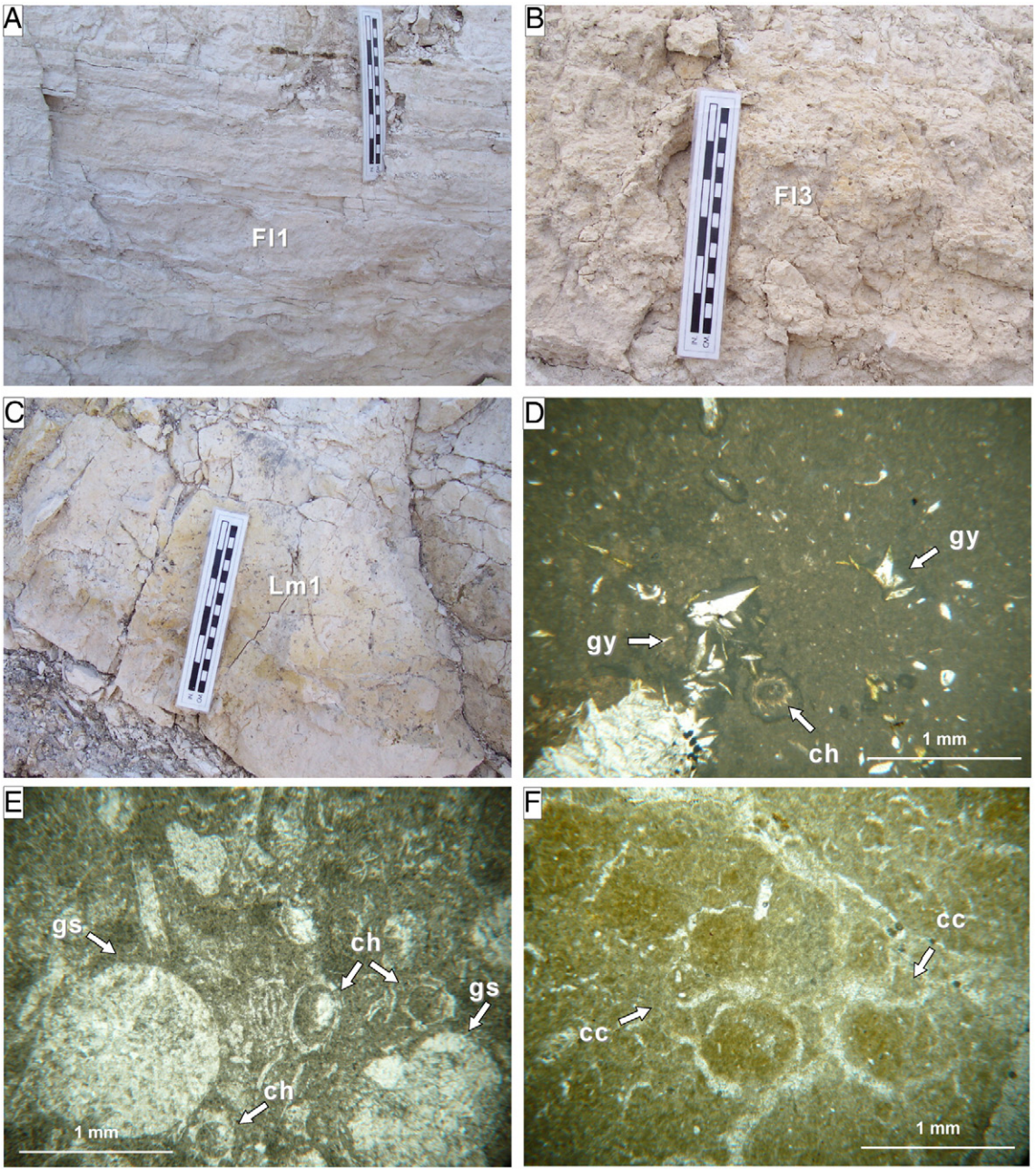

Fig. 6. Facies of the Karacaören Formation (FA2a; see Fig. 2 for locations); (A) Laminated marlstone (Fl1); (B) Massive mudstone (Fl3); (C) Clayey limestone (Lm1); (D) Wackestone texture of Lm1 facies with a micritic matrix, diffuse individual or composite rosette pseudomorphs and charophytes; (E) Packstones textures of Lm1 displaying micritic matrix and diffuse gastropod shells (gs) and calcified charophyte stems (ch); and (F) Circumgranular desiccation cracks (cc) in a packstones groundmass of Lm1.

microsphere and nanosphere crystals display granular surface and ragged outlines due to the grouping of small rhombohedrons (Fig. 7D). The second habit of dolomite in facies Lm2 is non-stoichiometric, Ca-rich (50–55% Ca, mean 54%) and poorly ordered (0.06 to 0.60, mean 0.34). Illite in facies Lm2 samples occurs as fibers and films, with aggregates forming micron-sized (up to 100 μm long) filaments that envelope subhedral to rhombohedral dolomite crystals (Fig. 7D).

4.2.1.1. Interpretation. The remarkable lateral continuity of the mudstone–marlstone–clayey limestone/dolostone alternations indicates that deposition took place in a low-gradient, shallow lake environment. Clayey limestone (Lm1) and marlstone (Fl1, Fl2) facies are interpreted as settling out of higher Ca-rich suspended and dissolved load to the lake during high lake level periods (Meléndez et al., 2009). The predominance of mudstone to wackestone textures indicates that the deposition of Lm1 and Lm2 carbonates occurred in a low-energy lacustrine environment (Alonso-Zarza et al., 2011). Pedogenic features (i.e. brecciation, nodularization, cracking, coated grains) suggest that littoral lake areas were subaerially exposed (Freytet and Plaziat, 1982; Alonso-Zarza, 2003). The good preservation of calcified charophyte stems also suggests that these sediments were deposited at shallow water depths (usually less than 10 m) and under low-energy conditions, which favor growth of these green algae (Anadón et al., 2000).

Clayey dolomites (Lm2) were probably deposited during episodes of increased supplies of mud and Mg-rich solution from the weathering of dolomitic limestones and metamorphic rocks containing Mg silicates in

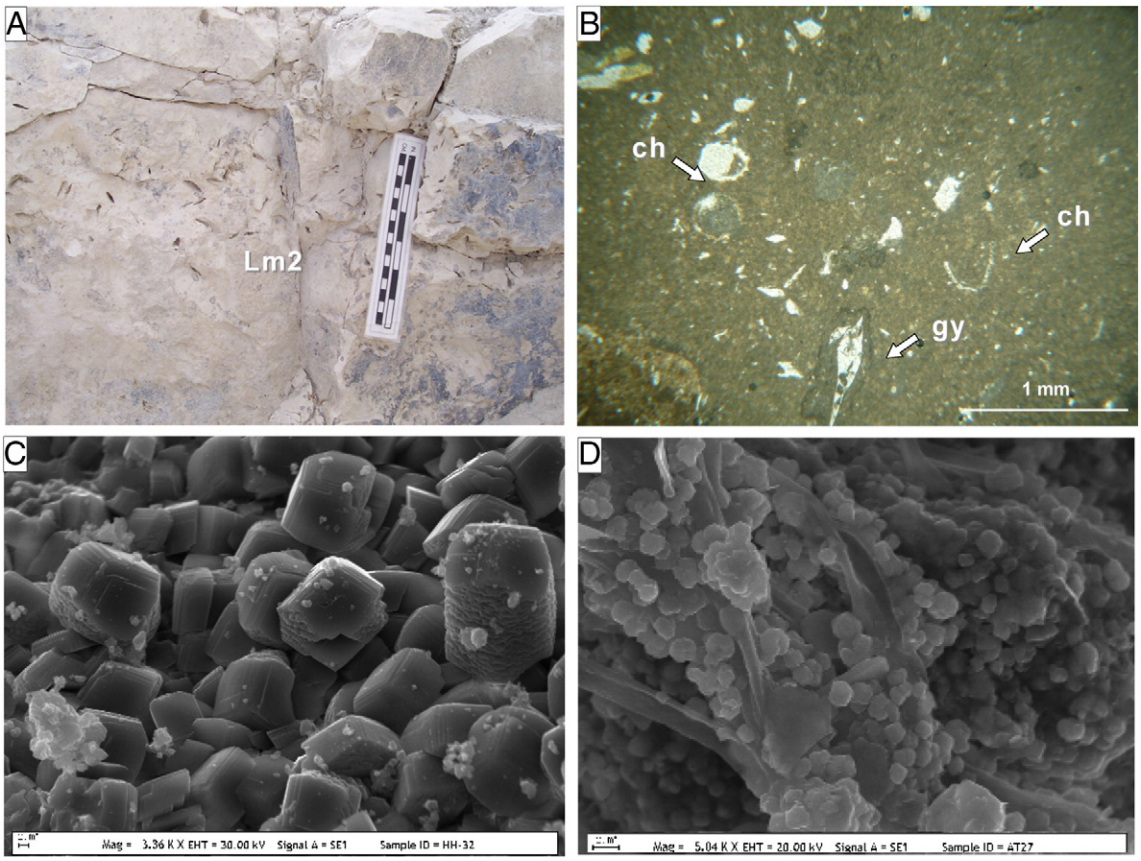

Fig. 7. Facies and photomicrographs from thin sections of clayey dolomite facies (Lm2) from the Karacaören Formation (FA2a; see Fig. 2 for locations); (A) Lenticular gypsum cast-bearing clayey dolomite (Lm2); (B) Mudstone texture of Lm2 with individual gypsum crystals (gy) and calcified charophyte stems (ch); (C) Subhedral to rhombohedral dolomite crystals (4–8 μm in size), and (D) The dolomite crystals formed by aggregates of microspheres vs. nanospheres (0.5–1.5 μm in size) and illite fibers and films.

the catchment area (Anadón and Utrilla, 1993). The subhedral to rhombohedral crystals (the second habit) of the Lm2 are interpreted as detrital in origin, whereas dolomite micro- and nano-crystals (the second habit) most likely resulted from primary precipitation in a shallow lake (Calvo et al., 2003). Petrographic and mineralogic features, such as the homogeneous compositional and textural character of the dolomite, the absence of replacement textures (i.e. syntaxial, submicron calcite domains in the dolomite), and Ca-rich and poor ordering support a direct primary origin for the dolomites (García del Cura et al., 2001; Sáez and Cabrera, 2002). The composition, size, morphology and spatial organization of the microsphere and nanosphere-shaped dolomites resemble those described by Bréhéret et al. (2008) and Sanz-Montero et al. (2008) from Holocene and Miocene lakes, respectively, where bacterially-induced dolomite is forming and/or formed in the past. The first habit of dolomite is interpreted to be of detrital origin. Gypsum pseudomorphs within carbonate beds (Lm1, Lm2) are usually interpreted as a result of early diagenetic interstitial precipitation from saline pore-fluids (Arenas et al., 1999). The formation of the gypsum crystals can be interpreted as a result of crystallization in littoral deposits, either in the phreatic or capillary zones (Salvany et al., 1994). The layers of massive mudstone (Fl3) separating carbonate beds are attributed to lake flooding episodes (Sáez and Cabrera, 2002).

4.2.2. Subassociation FA2b

This subassociation conformably and abruptly overlies the FA2a deposits and passes upward and laterally into FA2c deposits (Fig. 3). The FA2b deposits consist of black shales (facies Fl4), gray marlstones (facies Fl5), and bioclastic dolomites (facies Lm3). The subassociation is 55 m thick, occurs in the middle part of the Karacaören Formation, and is particularly well developed near the southern margin of the basin (see the Dandalas section in Fig. 4E and Karacaören 1 section in Fig. 4F). All facies are rich in euryhaline ostracodes (*Candona angulata*; *C. candida*, *C. neglecta* "*diktyota*", *C. neglecta* "*megala*"; *Cyprinotus incongruens*; *C. salinus salinus*; *Cypris* sp.; *Ilyocypris bradyi*, *I. gibba*, Becker-Platen, 1970) and brackish-water diatom species (i.e. *Achnanthes parvula*, *Rhopalodia operculata*, *Cocconeis placentula*, *Nitzschia macilenta*; Açıkalın, 2005).

Black shales (facies Fl4) display dark gray to black color and consist of claystones with thin bituminous laminae (1–5 mm thick; Fig. 8A). They form tabular to slightly lenticular beds 30 cm to 150 cm thick and several tens of meters in lateral extent. This facies is interbedded with bioclastic dolomite (Lm3) and gray laminated marlstone (Fl5). Usually, the black shales contain scattered lenticular gypsum crystals (3–7 mm in size), sulfur nodules (5–25 cm thick), ostracodes, diatoms (*C. placentula*), algae, and pollen. The calcite is predominantly microcrystalline and is composed of regular subhedral to euhedral crystals up to 10 μm in size. The associated dolomite is similar to those of facies Lm2 and consists of microsphere (1–1.5 μm) and nanosphere clusters (<1 μm in size) with spheroid hollow cores. The dolomite is Ca-rich (51–57%, mean 53%), and poorly ordered (0.20–0.62, mean 0.38). The shale samples are rich in organic matter, in which the total organic carbon (TOC) ranges from 0.75 to 14.58% (mean of 3.34).

Gray marlstones (facies Fl5) are dark gray to brown color and form tabular to slightly lenticular beds that are 30 cm to 200 cm thick and several tens of meters in lateral extent (Fig. 8B). They are massive, rarely parallel-laminated, and contain sulfur nodules, ostracodes, molluscs, and organic matter. This facies alternates with black shale (Fl4) and bioclastic dolomite (Lm3). Bioclastic dolomites (facies Lm3) are beige yellow to light brown, and well-cemented, forming massive tabular beds 10–100 cm thick (Fig. 8C) and alternating with black shale (Fl4) and gray marlstone (Fl5). They are texturally

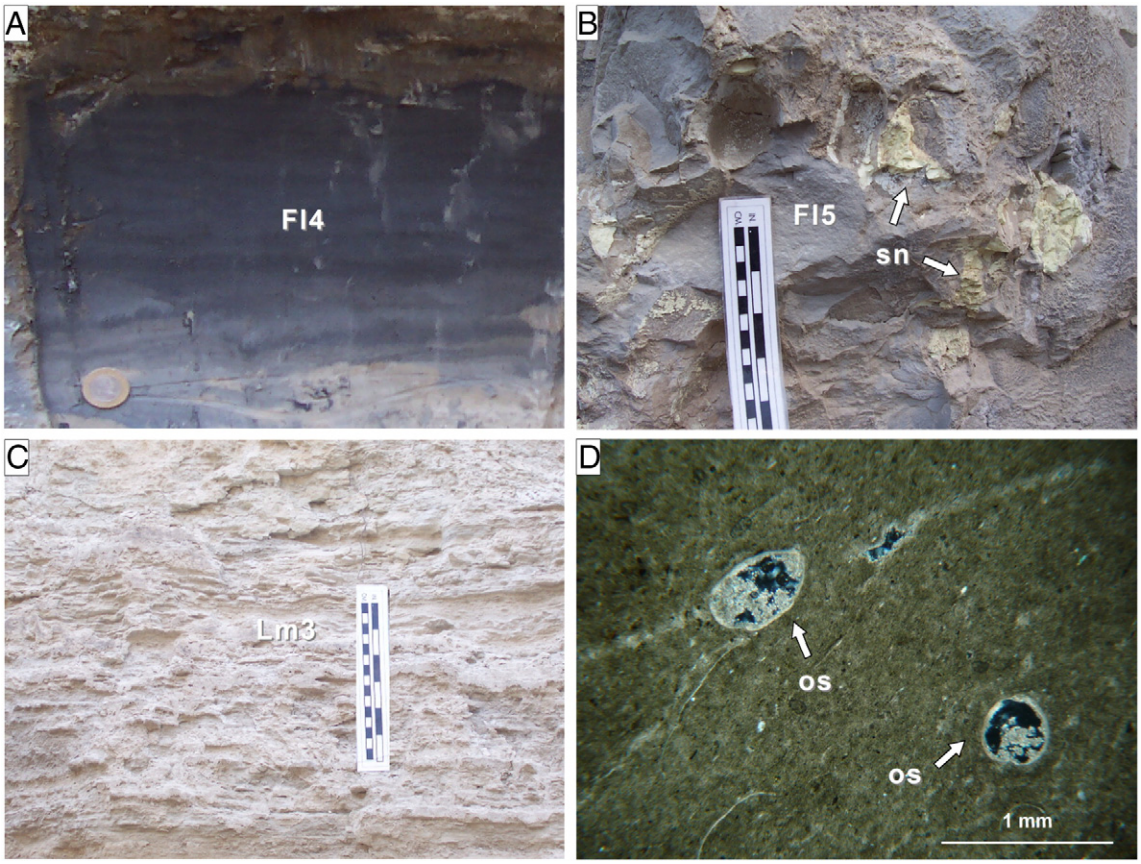

Fig. 8. Examples of open lake facies association from the Karacaören Formation (FA2b; see Fig. 2 for locations); (A) Black shale (Fl4) (Coin is 2 cm in diameter); (B) Sulfur nodule-bearing (sn) gray marlstone (Fl5); (C) Bioclastic dolomite facies (Lm3); and (D) Wackestone texture of bioclastic dolomite facies (Lm3) with a homogeneous micritic matrix with ostracodes (os).

wackestones to packstones composed of homogeneous micrite with poorly preserved ostracode shells (Fig. 8D). Shell cavities are filled with microsparite.

4.2.2.1. Interpretation. Subassociation FA2b was formed in an alkaline saline lake depositional environment, as shown by its fine grain size, preservation of fine lamination, presence of abundant euryhaline ostracodes, brackish water diatoms, and euryhaline algae (see section below). This interpretation is also supported by the lateral continuity of strata, and its geometry and relationships with the other facies associations. The occurrence of gypsum and sulfur-bearing, well-laminated facies, and the good preservation of organic matter indicate that the lake water column was alkaline saline perennial (Sáez et al., 2003; Paz and Rossetti, 2006). The presence of sulfur nodules within the black shales indicates production of hydrogen sulfide during bacterial sulfate reduction. Sulfate-reducing bacteria use sulfate to oxidize organic matter, which produces reduced hydrogen sulfide (Anadón et al., 1992). Microorganisms under anoxic conditions can use H_2S produced by sulfur-reducing bacteria and photosynthetic activity leads to sulfate ion production. This process leads to increased concentration of sulfate ions at the water–sediment interface and/or in the sediment. The released sulfate ions would combine with calcium ions to form gypsum (Verrecchia, 2007). Numerous studies have reported that sulfate-reducing bacteria directly induced dolomite precipitation in a variety of environments (e.g. Bréhéret et al., 2008; Sánchez-Román et al., 2008). Submicron-sized spherical to elliptical dolomite grains have been reported from both laboratory experiments and natural lake environments (e.g. García del Cura et al., 2001; Sanz-Montero et al., 2009). In all these cases, formation of dolomite was considered to be bacterially-induced. Sulfate reduction leads to the release of free Mg^{+2} ions from neutral ion pairs, leading to the precipitation of dolomite in the presence of the released HCO_3^- and Mg^{+2} ions (Deng et al., 2010). Hollow structures can be interpreted as mineralized extracellular polymeric secretions (EPS) that typically embed the microbial communities in mats and biofilms as suggested by Sanz-Montero et al. (2008). These microbial mats probably formed on the lake floor in which the decomposition of organic matter occurred (Sanz-Montero et al., 2008).

The bioclastic dolomites (facies Lm3) with wackestone–packstone textures are generally characteristic of low energy, open lake conditions. These dolomites most probably formed by direct precipitation, similar as facies Lm2 dolomites. The gray marlstones represent a low-energy environment dominated by muddy suspension fallout (Arenas and Pardo, 1999).

4.2.3. Subassociation FA2c

These deposits form the upper part of the Karacaören Formation and are well exposed in the northern part of the basin (see the Karacaören 2 section in Fig. 4G and Dedeler section in Fig. 4H). This assemblage consists of alternating massive (pebbly) sandstones (facies Sm1), laminated and clayey marlstones (facies Fl1 and Fl2), cherty marlstones (Fl6), cherty diatomites with minor gypsum (Fl7), clayey limestones and dolomites (Lm1 and Lm2), and cherty limestones (Lm4). These deposits are 55 m thick, overlie FA2b (Fig. 3), and extend laterally over tens of kilometers.

Massive (pebbly) sandstone (Sm1), laminated and clayey marlstones (Fl1 and Fl2) and clayey limestone (Lm1) and dolomite (Lm2) facies are similar to those of shallow lake deposits (FA2a) (Table 1). Cherty marlstones (Fl6) show white to beige color and form tabular to slightly lenticular beds 20 cm to 150 cm thick and several tens of meters in lateral extent. They are parallel-laminated or massive, and contain chert nodules (Fig. 9A). Cherty diatomites (Fl7) are beige to brown, parallel-laminated (0.3–0.9 cm in thickness), rarely massive,

and form tabular to slightly lenticular beds that are 30 cm to 150 cm thick and several tens of meters in lateral extent. They contain chert nodules (Fig. 9B) and only rare, poorly preserved, brackish-water diatom frustules (*A. parvula*; Fig. 9C). These diatomites mainly consist of quartz (mean 45%), opal-CT with minor opal-A (mean 8%), feldspar (mean 23%), dolomite (mean 2%), gypsum (mean 1%), sulfur (mean 5%) and clay minerals (mean 16%; smectite, illite, and kaolinite).

Cherty limestones (Lm4) are beige to yellow and well-cemented, forming massive tabular beds 30–150 cm thick, several tens of meters in lateral extent (Fig. 9D; Table 1). They show mudstone to wackestone fabric with a homogeneous micritic matrix, diffuse rare ostracodes, circumgranular cracks, cracks infilled with micritic fragments with sparite cements, and small cavities (Fig. 9E). These cavities are open and rarely filled with microsparite.

Chert appears in the facies of marlstone (Fl6), diatomite (Fl7), and limestone (Lm4) as broadly similar, forming isolated nodules and/or nodular structure along the beds. The long axes of nodules are oriented parallel to the bedding. There are sharp boundaries between nodule and associated limestone/diatomite/marlstone. Most of the chert nodules consist of a 3–20 cm thick, white or brownish gray porous texture with porcelain-like rinds and a black and dark brown striped thin core (Fig. 9A, B). In some of the chert nodules, wavy textures of bands and microbreccia textures are present. The lighter bands of the core are more porous than the darker ones. In general, smaller nodules reveal a simple pattern with a center (silicified intraclast or bioclast) coated with alternating siliceous bands terminated by a thicker porcelain-like rind, whereas larger nodules are far more complex with several separate centers. Under light microscopy, the

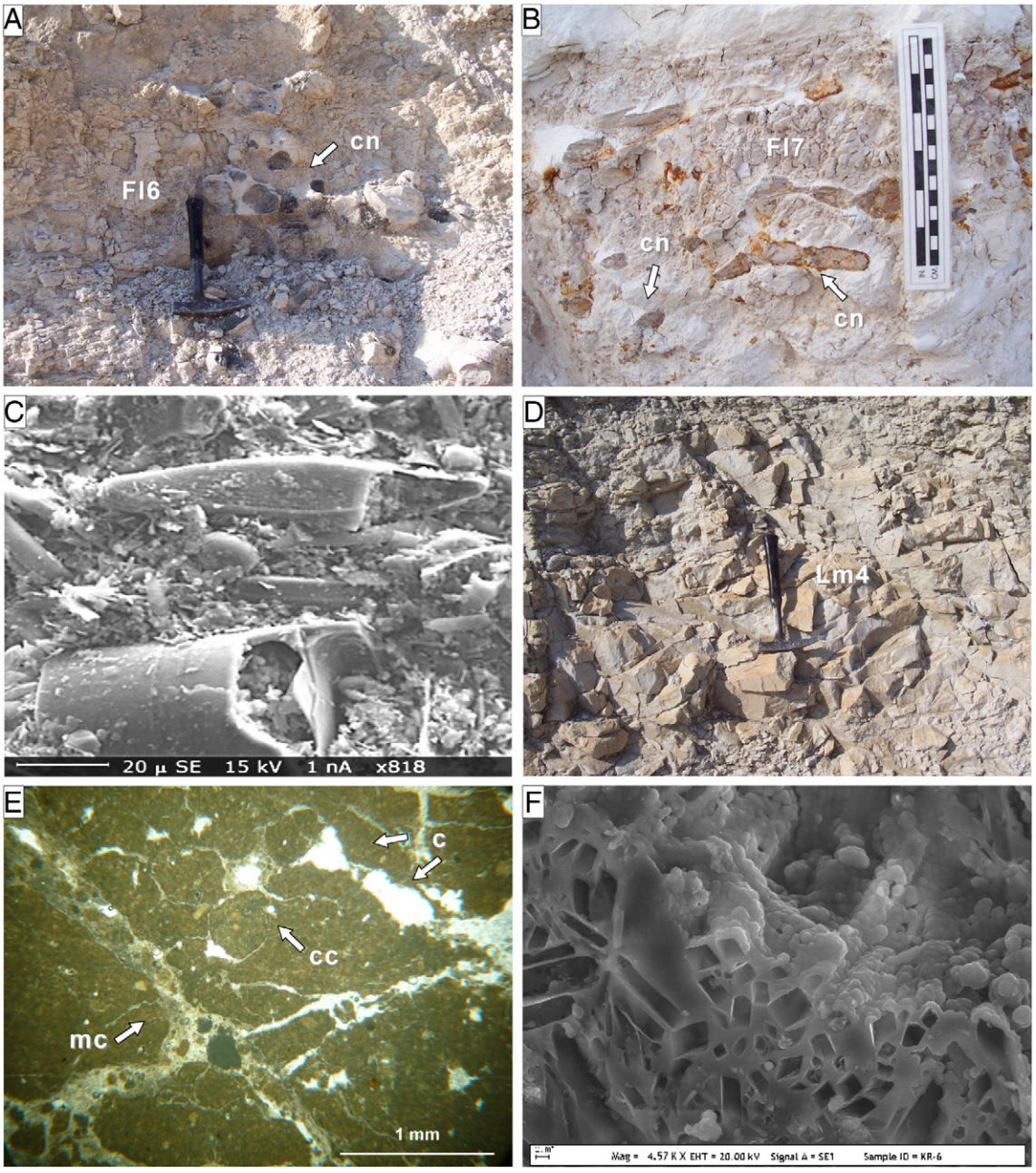

Fig. 9. Facies associations of the Karacaören Formation (FA2c; see Fig. 2 for locations); (A) Chert nodule-bearing (cn) marlstone (Fl6); (B) Chert nodule-bearing (cn) white to brown colored diatomite (Fl7); (C) SEM image of diatom (*Achnanthes parvula*) in the cherty diatomite; (D) Cherty dolomite (Lm4); (E) Circumgranular cracks (cc), mudcracks (mc) and cavities (c) in a mudstone groundmass of cherty limestone (Lm4); and (F) SEM images of cherts with small silica microspheres (1–3 µm in size) and angular quartz crystal casts (2–6 µm in size).

groundmass of the cherts largely consists of a mosaic of small anhedral quartz crystals. Under SEM, these cherts are very compact and it is difficult to observe crystals, but sometimes small silica microspheres (1–3 μm in size) and angular quartz crystal casts with a 2–6 micron diameter can be observed (Fig. 9F). These chert nodules include opal-CT with minor opal-A (mean 48%), quartz (mean 20%), dolomite (mean 12%), feldspars (mean 10%), calcite (mean 5%) and clay minerals (mean 5%). Dolomite in the Lm2 facies is non-stoichiometric, Ca-rich (49–58%, mean 55%) and poorly ordered (0.10 to 0.45, mean 0.33).

4.2.3.1. Interpretation. FA2c subassociation represents a lake margin environment. The micritic texture of the carbonate facies (Lm1, Lm2, and Lm4) and the presence of brackish-water diatom species and minor gypsum-bearing diatomites (Fl7) represent deposition in low-energy, alkaline to slightly saline, shallow lake margin environments. Subaerial exposure of micritic muds led to the development of cracks/fissures. The marlstone facies (Fl1, Fl2, and Fl6) reflect periods of raised lake levels combined with the supply of carbonate-rich muds from the weathering of the bedrock in the source area (Anadón et al., 1998). Massive (pebbly) sandstones (facies Sm1) reflect transitional siliciclastic/carbonate mudflats to a limy marsh to shallow lake deposition of carbonate (Gierlowski-Kordesch, 1998).

Kidder and Gierlowski-Kordesch (2005) demonstrated that the Miocene grass uptake of silica producing opaline phytoliths mobilized more silica in continental ecosystems from soils than pre-grass biogeochemical weathering processes. Consequently the gradual release of this relatively soluble silica along with other nutrients into rivers and lakes caused an to increase in diatom productivity. The cherty diatomites (Fl7) are interpreted as the result of the spread of grasslands and the increase of silica cycling in this basin. The poorly preserved diatom frustules and presence of opal-CT and quartz in the diatomites is thought to be result of silica diagenesis producing either opal-CT or quartz, indicating a highly alkaline diagenetic environment (Bustillo, 2010; Alonso-Zarza et al., 2011). Under these conditions, the amorphous, opaline silica of diatom frustules is progressively transformed to opal-CT and finally quartz to chert (Bustillo and Alonso-Zarza, 2007).

Cherts in limestone facies (Lm1, Lm4) and marlstone facies (Fl6, Fl7) formed under alkaline groundwater conditions (Armenteros et al., 1997). The silicification may have developed by the entering of siliceous groundwater moving slowly under high water table conditions within the carbonate flats towards the lake (Bustillo et al., 2002). Surface water can also contribute silica from grasses. A decrease in alkalinity due to inflow of groundwater with a relative low pH (<9) would have the formation development of chert (Bustillo and Alonso-Zarza, 2007). Both field and petrographic studies indicate that chert nodules are of synsedimentary-early diagenetic origin, supported by the following observations, such as the presence of brecciated texture in the chert nodules, the orientation of the long axis of all nodules is parallel to limestone, diatomite or marl beds, and the presence of sharp boundaries between nodule and associated limestone/diatomite/marl (Sharp et al., 2002).

4.3. Facies association III (FA3)

This facies association characterizes the Karacasu Formation, which is well exposed at the basin's southern margin, where it is cut by normal faults (e.g., the Karacasu fault in Fig. 2) and also unconformably overlies the metamorphic bedrock. Basinwards, it unconformably overlies the Karacaören Formation. Two facies subassociations (FA3a and FA3b) have been distinguished in the Karacasu Formation, which is similar to FA1a and FA1b of the Damdere Formation (Fig. 3).

FA3a subassociation forms the lower part of the Karacasu Formation and occurs in outcrops along the southern basin margin (see the Alemler section in Fig. 4I and Kızılyarbaşı section in Fig. 4J), where they are ca. 50 m thick and have a lateral extent of several hundreds of meters, thickening towards the basin-margin fault.

FA3b deposits are well represented in the Kızılyarbaşı section in Fig. 4J and Çamarası section in Fig. 4K, and are generally well developed in the central and northern part of the basin. This facies assemblage is up to 20 m thick, and can be followed northeastward over some kilometers, where it passes laterally into the deposits of FA3a towards the basin margin.

4.3.1. Interpretation

FA3a and FA3b deposits are interpreted as proximal–medial and distal alluvial fan as well in FA1a and FA1b of the Damdere Formation.

5. Stable isotopes and organic geochemistry

The results of stable isotope analyses of carbonate samples from five stratigraphic intervals of the basin-fill succession are listed in Table 2 and in Figs. 10 and 11.

Carbonate-rich calcrete samples from the FA1b facies subassociation (nodules of facies Fm) consist only of calcite with $\delta^{13}C$ values ranging from −6.81 to −5.45‰ PDB (mean = −6.33), whereas $\delta^{18}O$ values are variable and generally low, ranging from −9.05 to −7.15‰ PDB (mean = −8.18).

Carbonate deposits from FA2a facies subassociation comprise both calcite and dolomite and show a wide interval of ranges of $\delta^{13}C$ values. The variable $\delta^{13}C$ values for calcite (from −4.79 to −0.61‰ PDB; mean = −2.18) are lower than the dolomite (from −5.44 to +7.10‰ PDB, mean = −1.36). The $\delta^{18}O$ ratios are also variable and display more negative values for calcite (−9.21 to −4.19‰ PDB, mean = −6.67) than for dolomite (−5.30 to +2.73‰ PDB, mean = −1.05).

Carbonate deposits in FA2b subassociation, consisting of both calcite and dolomite, display narrow ranges of $\delta^{13}C$ values, which are broadly similar in both carbonates (−4.26 to +1.37‰ PDB for calcite, mean = −0.59; −1.74 to +1.18‰ PDB for dolomite, mean = −0.46). On the other hand, $\delta^{18}O$ ratios are highly variable and very similar in these carbonates (−8.79 to +5.89‰ PDB for calcite; mean = −1.99 and −8.47 to +5.04‰ PDB for dolomite; mean = −1.49). Black shale samples of the FA2b facies show wide ranges of $\delta^{13}C_{org}$ values (−26.96 to −18.96‰ PDB) (Table 3).

Carbonate samples of the FA2c facies subassociation mostly consist of dolomite with $\delta^{13}C$ values ranging from −2.94 to +3.82‰ PDB (mean = −0.49) and calcite with −1.98 to +1.11‰ PDB (mean = −0.54), which are quite similar to each other. The $\delta^{18}O$ ratios for calcite and dolomite show large variation, but are broadly similar (−0.63 to +2.53‰ PDB, mean = +0.81 and −3.35 to +3.82‰

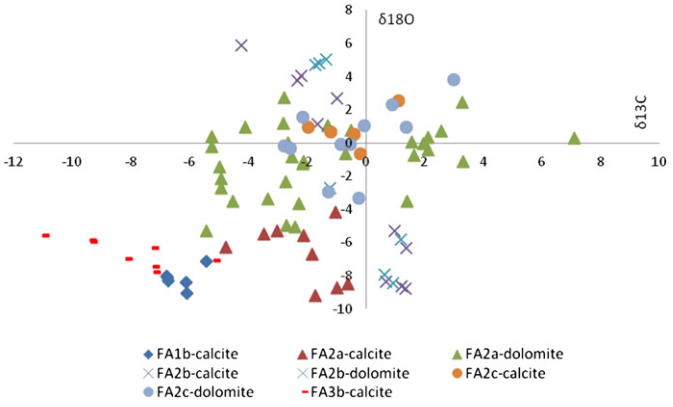

Fig. 10. Scatter plot of stable oxygen and carbon isotope ratios in carbonate samples from distal alluvial fan (FA1b and FA3b), shallow lake (FA2a), open lake (FA2b) and lake margin (FA2c) deposits of the basin-fill succession.

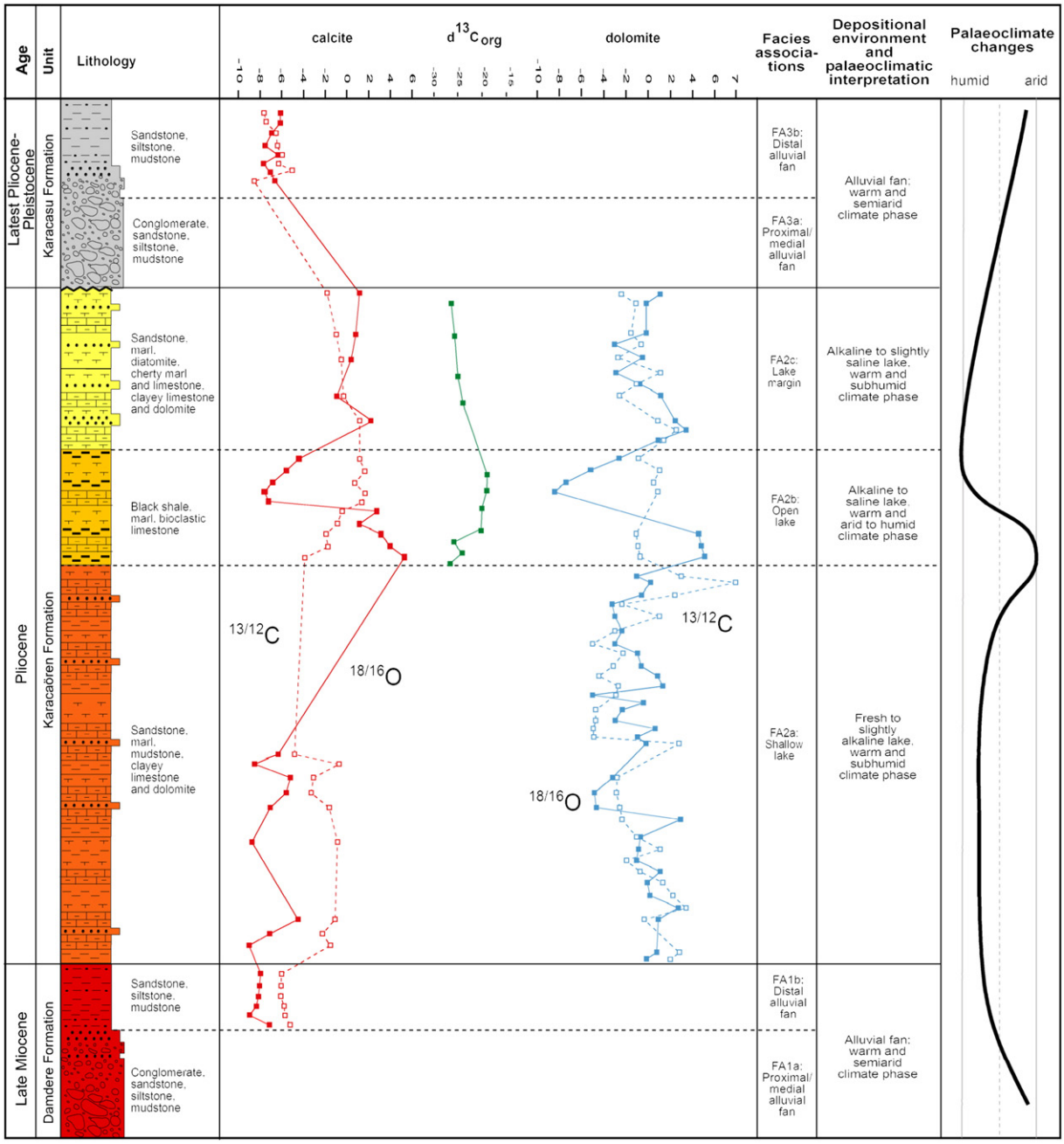

Fig. 11. Summary of the Neogene depositional history of the Karacasu Basin, including sedimentological, mineralogical and geochemical data and their paleoenvironmental interpretation (thickness not to scale).

Table 3
Total organic carbon (TOC) and organic carbon-13 values of various black shale and mudstone facies of Karacaören Formation in the Karacasu Basin.

Facies assoc.	Sample no.	Lithology	TOC (%)	$\delta^{13}C_{V\text{-}PBD}$ (‰)
Marginal lake FA2c	DE.14p	Mudstone	–	−26.26
	DE.12p	Mudstone	–	−25.68
	DE.10p	Mudstone	–	−24.57
	DE.8p	Mudstone	–	−24.27
Open lake FA2b	KRC.5p	Shale	1.43	−18.96
	KRC.3p	Shale	0.86	−19.13
	KRC.1p	Shale	1.11	−20.08
	DAN.7p	Shale	0.75	−20.26
	DAN.5p	Shale	2.44	−25.54
	DAN.3p	Shale	14.58	−24.13
	DAN.1p	Shale	2.23	−26.96

PDB, mean = +0.25, respectively). $\delta^{13}C_{org}$ values of FA2c are negative, ranging from −26.26 to −24.27‰ PDB (Table 2).

Carbonate-rich calcretes from FA3b consist only of calcite with $\delta^{13}C$ values ranging from −11.01 to −5.17‰ PDB (mean = −8.11), whereas $\delta^{18}O$ values are confined to a narrow range from −7.77 to −5.87‰ PDB (mean = −6.76).

6. Pollen analysis

Black shales (facies F14) belonging to the open lake deposits of the Karacaören Formation (Dandalas section: DAN 1, 3 and 5 and Karacaören-1 section: KRC 1 and 3 samples; Fig. 4E and F) bear a diverse pollen association (Fig. 12). Pollen spectra are characterized by high percentages of non-arboreal pollen (average ca. 75%), such as Poaceae

(around 40%), Amaranthaceae (around 10%), other Asteraceae (around 10%) and *Artemisia* (around 20% in the Dandalas section, Fig. 4E). The arboreal pollen assemblages (AP; between 10 and 40% of the pollen counts) are mostly characterized by *Quercus* (evergreen and deciduous) and *Pinus* (around 20% in the Karacaören-1 section, Fig. 4F). Other conifers such as *Abies*, *Cathaya*, *Cedrus*, Cupressaceae, and *Tsuga* occur in lower percentages. *Olea* and *Pistacia*, typical Mediterranean climate adapted taxa, also occur as well as riparian trees such as *Ulmus*, *Celtis*, *Alnus*, and *Betula*. Note the presence of *Engelhardia* and *Pterocarya* in the Dandalas (Fig. 4E) and Karacaören-1 (Fig. 4F) sections, respectively.

Pollen data from the two studied sections mostly differ in that the black shales in the Dandalas section (DAN 1, 3 and 5 samples) pollen spectra show higher percentages of *Artemisia* and Amaranthaceae. On the other hand, the Karacaören-1 (KRC 1 and 3 samples) pollen spectra are relatively richer in arboreal pollen species (10% higher), with *Pinus*, *Quercus* evergreen type and *Cathaya* as the most representative species, whilst *Artemisia* is lacking. Aquatic palynomorphs (freshwater algae *Botryococcus* and *Pediastrum*, and Cyperaceae) are very abundant in the Dandalas section (Fig. 4E) and are lacking from the KRC (Fig. 4F).

6.1. Interpretation

Vegetation around the Karacasu lake, during the deposition of the Dandalas deposits, was characterized as a steppe rich in Poaceae, *Artemisia*, Amaranthaceae, and Asteraceae (including other Asteraceae and Lactucaceae). Small patches of *Quercus* and *Pinus* trees probably grew at higher elevation. Riparian and other hygrophilous trees (*Ulmus*, *Alnus* and *Engelhardia*) were present on the lake shore, where water would be available all year long. The lake was deep, clear and its surface waters contained enough oxygen to support abundant colonies of photosynthetic algae such as *Botryococcus* and *Pediastrum* (Smittenberg et al., 2005). These freshwater algae live in very diverse lake environments from very oligotrophic waters to brackish (Smittenberg et al., 2005).

Environmental conditions changed during the deposition of Karacaören-1 sediments. A shallower lake is interpreted with few pollen data, indicating that vegetation around the lake changed as well. The most noticeable change is the lack of freshwater aquatic algae (*Botryococcus* and *Pediastrum*) in these samples, probably related to the lake shallowing (Jiménez-Moreno et al., 2011). Another noticeable variation is the change from a steppe to a more forested environment in the pollen spectra from the Karacaören-1 section (Fig. 4F). In general, all tree pollen species increased at that time (i.e., evergreen *Quercus*). For example, *Pinus* increased in ca. 20%; however, pollen studies in recent pine forests show that in locations where *Pinus* trees are present, *Pinus* percentages are nearly always 50–60% of the pollen sum (Andrade et al., 1994). As *Pinus* never reached percentages higher than 20% in this area (Fig. 12), they probably never grew anywhere close to the lake environment. Other montane conifers seem to increase at that time (see presence/absence data for *Tsuga*, *Cedrus* and *Abies* in Fig. 12).

In general, the abundant steppe vegetation indicated that the Karacasu Basin was characterized by an arid climate during the Pliocene. It was too dry in the lowlands to support a forest. Climate in Anatolia is well known for being arid since the Miocene (Popescu, 2006) and Anatolia is believed to be the source area for *Artemisia* for the rest of the Mediterranean area (Jiménez-Moreno et al., 2010). *Artemisia* became very abundant in the whole Mediterranean area at the end of the Pliocene, as the climate cooled and glacial–interglacial cycles appeared in the Northern Hemisphere (Combourieu Nevout and Vergnaud Grazzini, 1991; Joannin et al., 2007; Popescu et al., 2010). The presence of *Engelhardia* and *Pterocarya*, two thermophilous species (Jiménez-Moreno et al., 2005) that are extinct today from this area (Quézel and Médail, 2003), indicate that climate during the Pliocene was warmer than today. These are also very hygrophilous species and most likely grew on the lakeshore.

7. Discussion: paleogeographic evolution and paleoenvironmental changes of the Karacasu Basin

Most of the Neogene extensional grabens and half-grabens of southwestern Anatolia (Fig. 1) trend NW–SE (e.g., Denizli, Karacasu, Bozdoğan and Yatağan basins) and NE–SW (e.g., Söke, Çameli and Eşen basins). A few major grabens trending E–W in the western coastal zone (e.g., the Büyük Menderes Basin in Fig. 1) have been attributed to the N–S tectonic extension of the adjoining Aegean Sea region (Şengör et al., 1985; Mercier et al., 1989). Until recently, these latter grabens were considered to represent the Miocene initiation of post-orogenic extensional tectonics in western Anatolia.

Three major paleogeographic evolutionary stages can be established in the Karacasu Basin: (1) development of alluvial fan and fluvial systems during the late Miocene first stage of the basin; (2) establishment of a shallow to open lacustrine system in the basin center during the Pliocene with progradation of the lake margin deposits; and (3) fluvial incision and alluvial sedimentation by the latest Pliocene–Quaternary. The main chronological phases of the paleogeographic development of the basin and regional paleoclimatic changes are presented below.

7.1. Late Miocene

Basin subsidence began during the late Miocene (Roberts, 1988; Açıkalın, 2005). The basin began as a half-graben that was bounded by the southern major Karacasu normal fault (Fig. 2). The basin's depocenter was located close to the southwestern margin, and alluvial fan facies associations of the Damdere Formation formed (Fig. 13A). The northward progradation of alluvial systems resulted in the spread of proximal–medial (FA1a) and distal alluvial fan (FA1b) environments, and the basal FA1a deposits gradually passed upward into

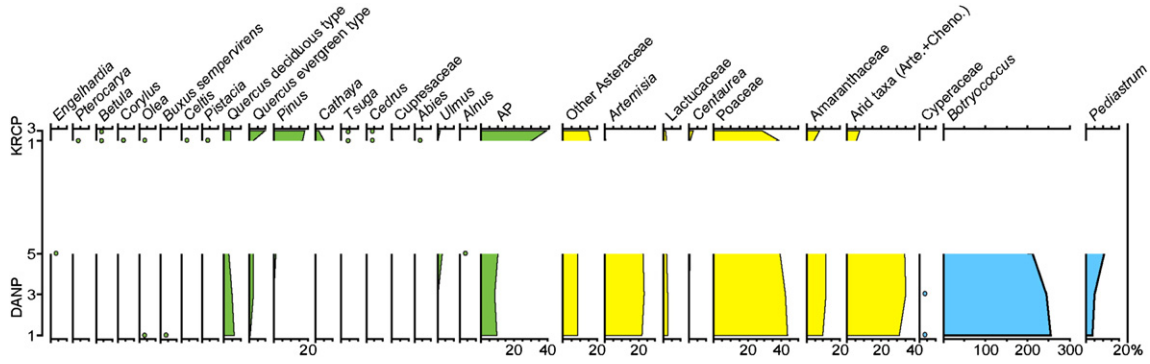

Fig. 12. Detailed pollen diagram from open lake deposits from the Dandalas (Fig. 3E) and Karacaören 1 (Fig. 3F) sections. Note that the distance between samples is not at scale. Dots represent percentages lower than 1%. In green are the trees and tall shrubs (with relatively high water requirements), in yellow the herbs and xerophytes (relatively lower water requirements) and in blue the aquatics.

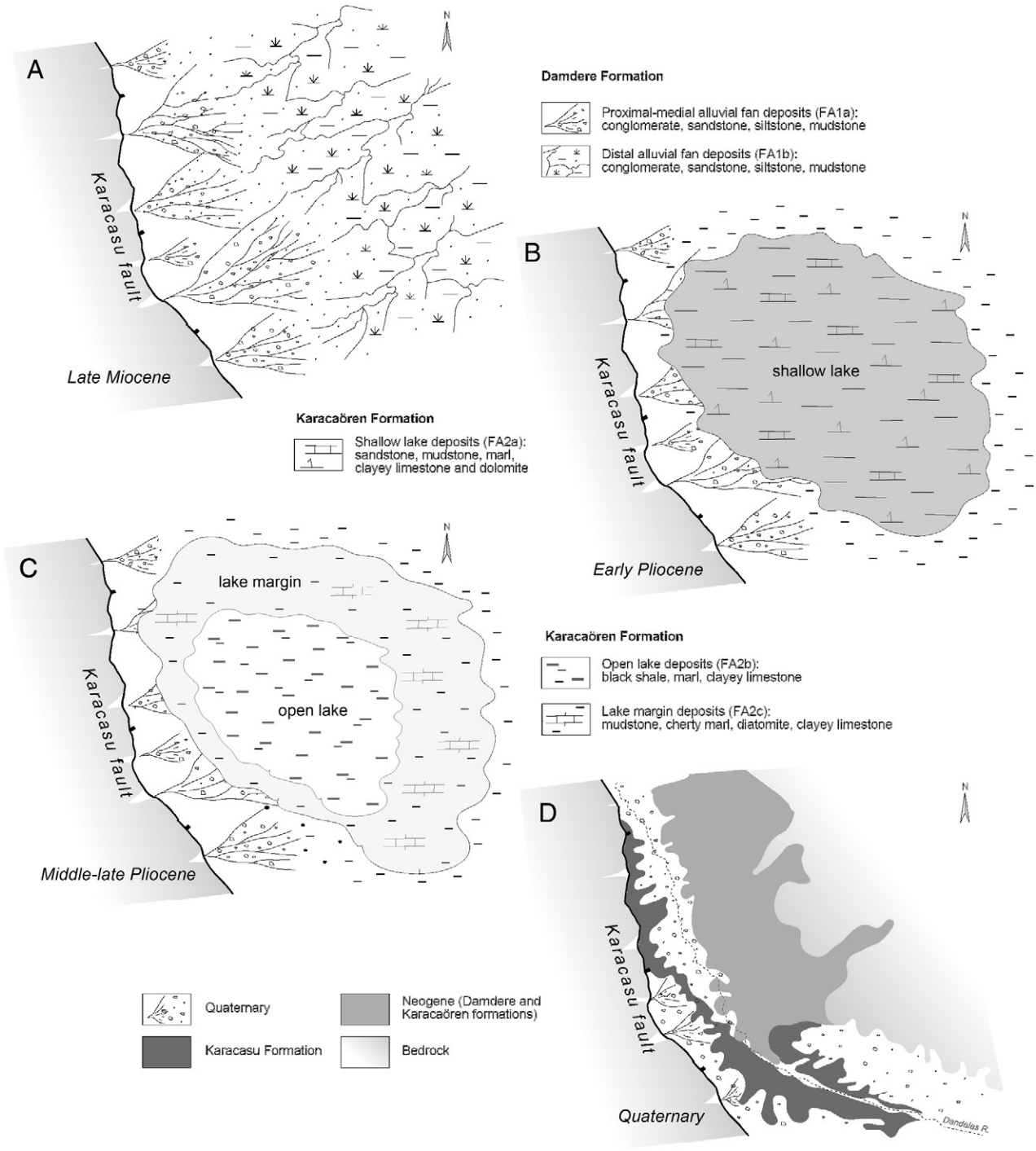

Fig. 13. Interpreted paleogeographic evolution of the Karacasu Basin. (A) The basin was formed by regional extension during the late Miocene, leading to deposition of the alluvial fan deposits (FA1a–b) of the Damdere Formation; (B) The basin was continued to subside accompanied by subhumid climate leading to deposition of the shallow lake deposits (FA2a) of the Karacaören Formation in the early Pliocene; (C) By the middle Pliocene arid to subhumid conditions to deposition of the alkaline to saline open lake (FA2b) that followed by subhumid climate caused to lake margin (FA2c) deposits of the Karacaören Formation in late Pliocene; and (D) By Quaternary the basin was dissected by the newly generated faults strands to the north that turned the half-graben basin into full-graben and leading to the deposition of the alluvial fan and fluvial deposits of the Karacasu Formation (FA3a–b) accompanied by semiarid conditions.

FA1b deposits. High accommodation space favored high level storage of isolated channels in floodplain sediments containing weak soil development (Alonso-Zarza, 2003). The presence of pedogenic fabrics (i.e. circumgranular fabrics, peloids) in the calcretes is indicative for pedogenesis (Alonso-Zarza, 2003). The morphology of calcretes reflects the different stages of their maturity and growth; therefore the nodular calcretes represent an early stage of calcretization and correspond to stages II to III as proposed by Machette (1985).

The low $\delta^{18}O$ isotope values of calcretes in FA1b (−9.05‰ to −7.15‰; mean = −8.18‰; Tables 2 and 4; Fig. 11) reflect isotopically light waters of meteoric origin (Huerta and Armenteros, 2005). This suggests that the calcretes were modified during meteoric diagenesis (Bustillo and Alonso-Zarza, 2007). The very negative $\delta^{13}C$ values may be related to high biogenic production of CO_2 in the soil zone (Talbot and Kelts, 1990; Alonso-Zarza, 2003). Similar deposits were described by Peryam et al. (2011) from the Plio-Pleistocene paleosols of

Table 4
Oxygen and carbon isotope values of the facies subassociations from the Karacasu Basin and their interpretation.

Facies subassociation	$\delta^{18}O$ (‰) calcite	$\delta^{13}C$ (‰) calcite	$\delta^{18}O$ (‰) dolomite	$\delta^{13}C$ (‰) dolomite	Interpretation
Distal alluvial fan — FA1b	−9.05 to −7.15	−6.81 to −5.45	–	–	Freshwater
Shallow lake — FA2a	−9.21 to −4.19	−4.79 to −0.61	−5.30 to +2.73	−5.44 to +7.10	Freshwater to slightly alkaline water
Open lake — FA2b	−8.79 to +5.89	−4.26 to +1.37	−8.47 to +5.04	−1.74 to +1.18	Alkaline to saline water
Lake margin — FA2c	−0.63 to +2.53	−1.98 to +1.11	−3.35 to +3.82	−2.94 to +3.82	Alkaline to slightly saline water
Distal alluvial fan — FA3b	−7.77 to −5.87	−11.01 to −5.17	–	–	Freshwater

the Fish Creek–Vallecito Basin and by Huerta and Armenteros (2005) from the Miocene calcretes of the Duero Basin. The strong $\delta^{18}O/\delta^{13}C$ covariance (correlation r-value = −0.80) shows a concomitant enrichment in ^{18}O and ^{12}C of the calcite. Pedogenic features (e.g. desiccation cracks, brecciation) of FA1b calcretes reflect semi-arid conditions.

7.2. Pliocene

At this time, lake level started to rise, and carbonate lake settings expanded to cover the entire basin (FA2a association, Karacaören Formation; Fig. 13B). Carbonate saturation of lake waters was favored by draining of a carbonate source area that in the Karacasu Basin corresponded to Karıncalıdağ Mountain. Benthic and planktonic autotrophic organisms such as cyanobacteria and algae contributed significantly to this productivity increase. These lacustrine zones were fed by surface runoff and groundwater contributions (through alluvial recharge zones) from surrounding ranges.

The abrupt shoreline shift towards the basin's margin may have been caused by an episode of the half-graben's increased asymmetrical subsidence, indicated by the presence of the NNW directed paleocurrents, and tilting of the basin floor accompanied by thickening of the beds toward the southern boundary fault (Karacasu Fault; Fig. 2). A similar tectono-sedimentary pattern has been observed in the Neogene basins of Denizli, Büyük Menderes, Bozdoğan, Çameli and Eşen nearby the Karacasu Basin (Fig. 1; Alçiçek, 2010). The overlying shallow lake deposits of FA2a are dominated by alternating clayey limestone and dolomite, marlstone, and mudstone, indicating installation of a broad and shallow, low-energy lake over the terminal fan area. Early diagenetic modification of the clayey limestones (Lm1) and dolomites (Lm2) leading to brecciation, planar and circumgranular desiccation cracks, and root traces occurred under evaporative conditions when the lake was gradually lowering and carbonates became exposed similar to that concluded by Arenas et al. (1999) from Miocene lacustrine deposits of the Ebro Basin, NE Spain. Late diagenetic features, i.e. lenticular gypsum casts in Lm1 and Lm2 facies indicate saline groundwater inputs which were related to subaerial exposure periods in the lake due to water level conditions (Sáez et al., 2007).

The negative $\delta^{18}O$ values of calcite in the FA2a facies subassociation (−9.21‰ to −4.19‰ for calcite, mean = −6.67‰; Tables 2 and 4; Fig. 11) indicate the input of ^{16}O-rich meteoric waters probably as result of a subhumid climate (Bustillo et al., 2002). The negative $\delta^{13}C$ values of calcite may reflect an involvement of isotopically light CO_2 derived from biological processes related to the pond vegetation, in addition to the supply of HCO_3^- by meteoric water drained from the surrounding groundwater table (Huerta and Armenteros, 2005). The relatively low $\delta^{18}O$ isotope ratios and the lack of significant $\delta^{18}O/\delta^{13}C$ covariance in FA2a (correlation r-value of 0.20 for calcite and 0.36 for dolomite) indicate a hydrologically open lake. Their mean isotopic values of the dolomites ($\delta^{18}O$ = −1.05‰ and $\delta^{13}C$ = −1.36‰) are clearly heavier than those of the calcites ($\delta^{18}O$ = −6.67‰ and $\delta^{13}C$ = −2.18‰). This indicates that the waters from which dolomite precipitated were more evolved (i.e. more influenced by evaporative conditions and/or residence time effects) than the waters from which calcite precipitated (Anadón and Utrilla, 1993). The $\delta^{13}C$ values of the dolomites, heavier than those of the calcites, indicate an effect of increased contribution of atmospheric CO_2 to the reservoir of dissolved carbon (Mayayo et al., 1996).

The freshwater to slightly alkaline lake (FA2a) of the Karacaören Formation became replaced by a relatively anoxic, open and alkaline to saline lake (FA2b association). These conditions are most common in balanced-fill lake, characterized by the rates of sediment/water supply in balance with potential accommodation (Fig. 13C; cf. Bohacs et al., 2000). The thickening of FA2b deposits in the southwestern basin margin points to longer persistence of open lacustrine settings. Rhythmic alternations of bituminous shale, clayey dolomite, and marlstone suggest that during the deposition of organic-rich intervals, the lake was relatively deep and developed stable water stratification, combined with low decay of organic matter, with dysoxic or anoxic bottom conditions (Ramos et al., 2001; Sáez and Cabrera, 2002). This is supported by the good pollen preservation in the black shales, pointing to low oxygen and thus low degradation of organic matter on the lake bottom. The dark gray colored marlstone and dolomite facies record the maximum carbonate mud input from the marginal lake zone to the inner basin. The generation of black shales was likely favored by presence of clay-rich source rocks. Deposition of black shales took place in a high-salinity, density-stratified, anoxic lake environment. The widespread occurrence of well-laminated facies and the good preservation of organic matter indicate a lake water column that was perennial and deep enough to allow long-term water stratification (meromixis) (Jiang et al., 2006). Similar deposits are described by Anadón et al. (1992) from the Miocene lacustrine deposits of the Teruel Graben and by Valero-Garcés and Kelts (1995) from the Holocene Medicine Lake Basin.

The mean $\delta^{18}O$ values of the dolomites (−8.47‰ to +5.04‰, mean = −1.49‰) and calcites (−8.79‰ to +5.89‰, mean = −1.99‰; Tables 2 and 4) are quite similar and indicate that calcite and dolomite precipitated in similar conditions. The slightly negative to positive $\delta^{13}C$ values of the calcites (−4.26‰ to +1.37‰, mean = −0.59‰) and dolomites (−1.74‰ to +1.18‰, mean = −0.46‰; Tables 2 and 4) are similar and reflect a relatively high primary production in the lake or non-equilibrium outgassing of ^{12}C to the atmosphere upon prolonged evaporative evolution of the lake (Talbot, 1990). ^{13}C enrichment in early diagenetic carbonates is also related to bacterial methanogenesis (Talbot, 1990) and diagenetic production of isotopically heavy ^{13}C due to bacterial methanogenesis in anoxic settings or isotopically light ^{12}C from bacterial sulfate reduction (Talbot and Kelts, 1990).

The isotopic trend of the FA2b has a strong negative covariance (correlation coefficient r = −0.94 for calcite, r = −0.90 for dolomite), which indicated a long residence for water in a hydrologically closed lake (Talbot, 1990; Anadón et al., 2000). The negative covariance is explained by concomitant enrichment in ^{18}O and ^{12}C, suggesting decrease in the freshwater input and evaporative effects generate an enrichment of ^{18}O and in organic productivity can lead to ^{12}C enrichment (Utrilla et al., 1998). A similar negative covariance was recorded by Valero-Garcés and Kelts (1995) in meromictic, saline lake deposits from the Holocene Medicine Lake basin.

The more positive $\delta^{18}O$ values of the overlying FA2b deposits (+5.89‰ to −5.30‰ for calcite; Tables 2 and 4; Fig. 11) indicate decreasing salinity and change from arid to relatively more humid climatic conditions. This is supported by the pollen record that shows a change from an *Artemisia*-steppe environment (Dandalas section) to a more forested (higher arboreal pollen (AP) percentages) and "grass dominated" environments (Karacaören-1 section) (Fig. 12).

Simultaneously, $\delta^{13}C$ ratios decreased, thus reflecting lower organic productivity and the input of ^{12}C-enriched CO_2 from decayed organic matter (Talbot, 1990). This is indicated by an upward decrease in abundance of algae in these deposits (Fig. 12).

The vegetation change observed from an *Artemisia*-steppe environment to a more forested and "grass dominated" steppe environment between the Dandalas and Karacaören-1 sections (FA2b; Figs. 3E, F and 12) can be explained by a climate change from cold and dry (i.e., glacial) to relatively warm and wet (i.e., interglacial). Similar changes have been observed in a long Pliocene pollen record from the Black Sea (DSDP site 380; Popescu et al., 2010), relatively close to the Karacasu Basin. The shallowing of the lake (from Dandalas to Karacaören-1 sections), due to sediment filling or by tectonics, would produce increasing levels of stress in the algae community (*Botryococcus* and *Pediastrum*) and would generate the loss of these species that grow well in deep and oligotrophic waters (Smittenberg et al., 2005; Jiménez-Moreno et al., 2011).

A change toward less negative values is observed in the $\delta^{13}C_{org}$ at the top of the Dandalas and Karacaören-1 sections (Fig. 11, Table 3). Values between −26 and −24‰ fall in the less-negative range of terrestrial C3-plants (trees and shrubs) or lacustrine algae (Meyers and Lallier-Vergès, 1999; Sáez and Cabrera, 2002). A trend toward less negative values is observed towards the top of the Dandalas section (Fig. 4E; reaching −20.26‰). Values seem to stabilize in the Karacaören-1 section (Fig. 4F; around −19‰). This could be explained by the fact that algae (*Botryococcus* and *Pediastrum*) are lacking in the sediments from the Karacaören-1 section (see pollen diagram in Fig. 12). Alternatively, this change could be explained by a greater presence of C4 grasses on the landscape (note the abundance of grasses in the pollen diagram; Fig. 12). However, this later hypothesis would be in disagreement with the pollen results that show a higher development of forest and the interpretation of a warmer/wetter climate in the area. Also, this wide range (i.e. 8‰) of $\delta^{13}C_{org}$ values could reflect early diagenesis of FA2b carbonates under varying mixtures of atmospheric and soil-derived CO_2 from the surrounding catchment area, as suggested by Sáez and Cabrera (2002).

The deposits of facies association FA2b pass vertically and laterally (see Fig. 3), towards the basin margin, into a sequence of alternating clayey/cherty limestone and dolomite, sandstone, marlstone, abundant chert and minor gypsum-bearing diatomite deposits of association FA2c, recording more frequent episodes of subaerial exposure (Fig. 13C). Occurrences of these carbonates reflect calcium and magnesium-rich, alkaline to slightly saline waters. Ca and Mg ions would have been supplied from the upland drainage of carbonate bedrock. The inflow of silica-saturated groundwaters into an alkaline lake would have caused changes in the hydrological conditions, leading to silica precipitation. The cherty limestones modified by syndepositional diagenetic processes (silicification), suggesting groundwater inputs during periods of high lake levels (Arenas et al., 1999). Cryptocrystalline cherts were probably precipitated directly by an influx of Si-rich groundwaters into an alkaline lake (Bustillo et al., 2002). FA2c deposits filled with the accommodation space created by subsidence, leading to a balance between sediment supply and subsidence. Periodic changes in the lake level caused episodic desiccation and pedogenic alteration of the lake-margin deposits.

The slightly negative to positive $\delta^{18}O$ values of the FA2c deposits (−0.63‰ to +2.53‰ for calcite and −2.94‰ to +3.82‰ for dolomite; Tables 2 and 4; Fig. 11) indicate subhumid climatic conditions. The negative $\delta^{18}O$ values and the weak positive covariance between the carbon and oxygen isotope values are interpreted as the result of hydrologically open lake ($r = 0.41$ for calcite, $r = 0.51$ for dolomite). These signals may reflect groundwater diagenesis. Average isotopic values of the dolomites ($\delta^{18}O = +0.25$‰ and $\delta^{13}C = -0.49$‰) and calcites ($\delta^{18}O = +0.81$‰ and $\delta^{13}C = -0.54$‰) are broadly similar. The slightly negative to positive $\delta^{13}C$ isotope ratios in the facies association FA2c reflect the effect of light-CO_2 extraction due to the photosynthetic activity of plants (Dunagan and Driese, 1999).

7.3. Latest Pliocene–Quaternary

At this time, the lake accommodation space was eventually exhausted. This is indicated by the basin-wide expansion of fluvial sedimentation and erosional deposition of facies association FA3. The increased rate of fluvial sediment supply exceeded the rate of accommodation creation in the lacustrine basin. Tectonic subsidence persisted, as indicated by the considerable cumulative thickness and multi-story paleochannel architecture of the fluvial succession.

Subsidence decreased substantially to produce a fluvial basin (cf. Bohacs et al., 2000), and the Karacasu Basin turned into a full-graben by newly generated intrabasinal faults (Fig. 13D) leading to the establishment of marginal alluvial fans and axial rivers of the early Quaternary Karacasu Formation (FA3 facies association), which overlies the Neogene Dandalas group through an angular unconformity. The very negative $\delta^{18}O$ isotope ratios (−7.77‰ to −5.87‰, mean = −6.76‰; Tables 2 and 4; Fig. 11), the presence of strong $\delta^{18}O/\delta^{13}C$ covariance ($r = -0.75$) and the occurrence of desiccation cracks, root traces, and brecciation in calcrete facies of FA3b carbonates, altogether these features indicate semiarid conditions. The low $\delta^{18}O$ isotope values of calcretes in FA3b reflect input of ^{16}O-enriched waters of meteoric origin (Alonso-Zarza and Arenas, 2004). The very negative $\delta^{13}C$ isotope values (−11.01‰ to −5.17‰, mean = −8.11‰; Table 2; Fig. 11) indicate an influence of ^{12}C-enriched soil-derived meteoric water (Abdul Aziz et al., 2003; Dunagan and Turner, 2004). A similar trend for Plio-Quaternary transition was also recorded in Çal basin to northeast by Alçiçek and Alçiçek (in press).

The transformation of Karacasu Basin from a half-graben to a graben occurred synchronically as well in another basins to the west–northwest, such as in the Gediz, Büyük Menderes, and Denizli grabens (Fig. 1; Purvis and Robertson, 2005; Alçiçek et al., 2007; Gürer et al., 2009; Çiftçi and Bozkurt, 2010). Present-day sedimentation characterized by small alluvial fans has largely smoothed out the pre-existing topographic relief of the basin.

8. Conclusions

The Karacasu Basin contains a prominent Neogene record of depositional, paleoenvironmental and paleoclimatic changes. Sedimentation in the basin started during the late Miocene with the deposition of alluvial fan to fluvial environments (FA1; Damdere Formation). The lake was small at the early stage. In the early Pliocene, a shallow lake occupied the central part of the basin. The overlying shallow lake facies association (FA2a; Karacaören Formation) represents lake expansion running in parallel with shoreline fluctuations and frequent episodes of subaerial exposure. Later on, the fresh to slightly alkaline shallow lake of FA2a turned into an open meromictic lake (FA2b). At this stage the lake was characterized by stratified and anoxic waters in the deeper parts of the lake. A vegetation change, from an *Artemisia*-steppe environment to a more forested and "grass dominated" steppe environment in the FA2b lake sediments is documented by pollen analysis. This could be explained by a climate change from cold and dry (i.e., glacial) to relatively warm and wet (i.e., interglacial) conditions. A shallowing of the lake at that time could have caused, for various reasons (i.e., decrease in nutrients or dissolved oxygen and/or increase in turbidity), a reduction in primary productivity and the loss of aquatic algae, which is reflected in the isotopic $\delta^{13}C_{org}$ change towards values closer to C4 grasses. FA2b deposits passes upward into lake margin deposits of FA2c, which reflect alkaline to slightly saline, shallow lake with a highly fluctuating shoreline and frequent periods of subaerial emergence. At the Pliocene–Quaternary transition, lacustrine conditions ceased, which is a common feature observed in other continental basins of SW Anatolia and the modern graben architecture with alluvial and fluvial settings developed (FA3; Karacasu Formation).

Both sedimentologic and geochemical data point to remarkable changes in the hydrologic budget of the basin and provide evidence

for long- and short-term fluctuations of the lake level. The composition of terrigenous sediment and the chemistry of water supplied to the lake were controlled by the weathering, chemical leaching and erosion of the metamorphic and cherty carbonate bedrock in the basin's catchment area. This source rock yielded Ca- and Mg-rich carbonate solutions that caused the deposition of lacustrine carbonates in the lake systems developed in the basin.

Acknowledgments

This study was sponsored by the Scientific and Technical Research Council of Turkey (TÜBİTAK research grants ÇAYDAG 108Y097). GJM's research was supported by project CGL-2010-20857/BTE of the Ministerio de Educación y Ciencia of Spain and the research group RNM0190 of the Junta de Andalucía. We thank G.J. Weltje, E.H. Gierlowski-Kordesch and J.P. Calvo for their constructive and helpful comments that improved the manuscript.

References

Abdul Aziz, H., Sanz-Rubio, E., Calvo, J.P., Hilgen, F.J., Krijgsman, W., 2003. Palaeoenvironmental reconstruction of a Middle Miocene alluvial fan to cyclic shallow lacustrine depositional system in the Calatayud Basin (NE Spain). Sedimentology 50, 211–236.

Açıkalın, S., 2005. Sedimentary evolution of the Karacasu cross-graben (Aydın, West Anatolia). MSc Thesis Osmangazi Univ., Eskişehir, Turkey (In Turkish.).

Alçiçek, M.C., 2007. Tectonic development of an orogen-top rift recorded by its terrestrial sedimentation pattern: the Neogene Eşen Basin of southwestern Anatolia, Turkey. Sedimentary Geology 200, 117–140.

Alçiçek, M.C., Ten Veen, J.H., 2008. The late Early Miocene Acipayam piggy-back basin: refining the last stages of Lycian nappe emplacement in SW Turkey. Sedimentary Geology 208, 101–113.

Alçiçek, H., 2009. Late Miocene nonmarine sedimentation and formation of magnesites in the Acıgöl Basin, southwestern Anatolia, Turkey. Sedimentary Geology 219, 115–135.

Alçiçek, H., 2010. Stratigraphic correlation of the Neogene basins in southwestern Anatolia: regional palaeogeographical, palaeoclimatic and tectonic implications. Palaeogeography, Palaeoclimatology, Palaeoecology 291, 297–318.

Alçiçek H., Alçiçek M.C., in press. Palustrine carbonates and pedogenic calcretes in the Çal basin of SW Anatolia: implication on the Plio-Pleistocene regional climatic turnover in the Eastern Mediterranean. Catena http://dx.doi.org/10.1016/j.catena.2013.03.010.

Alçiçek, H., Mayda, S., 2009. Sedimentological, mineralogical and geochemical investigation of the Karacasu Neogene Basin: an approach for the palaeogeographic and palaeoclimatic reconstruction (SW Anatolia, Turkey). Scientific Report No. ÇAYDAG 108Y097. Scientific and Technical Research Council of Turkey (TÜBİTAK), Ankara (144 pp.).

Alçiçek, M.C., Kazancı, N., Özkul, M., 2005. Multiple rifting pulses and sedimentation pattern in the Çameli Basin, southwestern Anatolia, Turkey. Sedimentary Geology 173, 409–431.

Alçiçek, H., Varol, B., Özkul, M., 2007. Sedimentary facies, depositional environments and palaeogeographic evolution of the Neogene Denizli Basin of SW Anatolia, Turkey. Sedimentary Geology 202, 596–637.

Alonso-Zarza, A.M., 2003. Palaeoenvironmental significance of palustrine carbonates and calcretes in the geological record. Earth-Science Reviews 60, 261–298.

Alonso-Zarza, A.M., Arenas, C., 2004. Cenozoic calcretes from the Teruel Graben, Spain: microstructure, stable isotope geochemistry and environmental significance. Sedimentary Geology 167, 91–108.

Alonso-Zarza, A.M., Genise, J.F., Verde, M., 2011. Sedimentology, diagenesis and ichnology of Cretaceous and Palaeogene calcretes and palustrine carbonates from Uruguay. Sedimentary Geology 236, 45–61.

Anadón, P., Utrilla, R., 1993. Sedimentology and isotope geochemistry of lacustrine carbonates of the Oligocene Campins Basin, north-east Spain. Sedimentology 40, 699–720.

Anadón, P., Rosell, L., Talbot, M.R., 1992. Carbonate replacement of lacustrine gypsum deposits in two Neogene continental basins, eastern Spain. Sedimentary Geology 78, 201–216.

Anadón, P., Robles, F., Roca, E., Utrilla, R., Vázquez, A., 1998. Lacustrine sedimentation in the diapir-controlled Miocene Bicorb Basin, eastern Spain. Palaeogeography, Palaeoclimatology, Palaeoecology 140, 217–243.

Anadón, P., Orti, F., Rosell, L., 2000. Neogene lacustrine systems of the southern Teruel Graben (Spain). In: Gierlowski-Kordesch, E.H., Kelts, K.R. (Eds.), Lake Basins Through Space and Time. AAPG Stud. Geol. 46, The American Association of Petroleum Geologists, Tulsa, pp. 497–504.

Andrade, A., Valdeolmillos, A., Ruíz-Zapata, B., 1994. Modern pollen spectra and contemporary vegetation in the Paramera Mountain range (Ávila, Spain). Review of Palaeobotany and Palynology 82, 127–139.

Arenas, C., Pardo, G., 1999. Latest Oligocene–Late Miocene lacustrine systems of the north-central part of the Ebro Basin (Spain): sedimentary facies model and palaeogeographic synthesis. Palaeogeography, Palaeoclimatology, Palaeoecology 151, 127–148.

Arenas, C., Alonso-Zarza, A.M., Pardo, G., 1999. Dedolomitization and other early diagenetic processes in Miocene lacustrine deposits, Ebro Basin (Spain). Sedimentary Geology 125, 23–45.

Armenteros, I., Daley, B., García, E., 1997. Lacustrine and palustrine facies in the Bembridge Limestone (Late Eocene, Hampshire Basin) of the Isle of Wight, southern England. Palaeogeography, Palaeoclimatology, Palaeoecology 128, 111–132.

Becker-Platen, J.D., 1970. Lithostratigraphische Unterschungen im Kanozoikum Südwest Anatoliens (Türkei) — Kanozoikum und Braunkohlen der Turkei. Beiheft. Geol. Jahrb., 97. Hannover (244 pp.).

Bohacs, K.M., Carroll, A.R., Neal, J.E., Mankiewwicz, P.Z., 2000. Lake-basin type, source potential, and hydrocarbon character: an integrated sequence-stratigraphic-geochemical framework. In: Gierlowski-Kordesch, E.H., Kelts, K.R. (Eds.), Lake Basins through Space and Time: AAPG Stud. Geol., 46, pp. 3–33.

Bozkurt, E., 2001. Neotectonic of Turkey a synthesis. Geodinamica Acta 14, 3–30.

Bréhéret, J.G., Fourmont, A., Macaire, J.J., Négrel, P., 2008. Microbially mediated carbonates in the Holocene deposits from Sarlième, a small ancient lake of the French Massif Central, testify to the evolution of a restricted environment. Sedimentology 55, 557–578.

Bustillo, M.A., 2010. Silicification of continental carbonates. In: Alonso-Zarza, A.M., Tanner, L.H. (Eds.), Carbonates in Continental Settings: Geochemistry, Diagenesis and Applications. : Developments in Sedimentology, 62. Elsevier, Amsterdam, pp. 153–178.

Bustillo, M.A., Alonso-Zarza, A.M., 2007. Overlapping of pedogenesis and meteoric diagenesis in distal alluvial and shallow lacustrine deposits in the Madrid Miocene Basin, Spain. Sedimentary Geology 198, 255–271.

Bustillo, M.A., Arribas, M.E., Bustillo, M., 2002. Dolomitization and silicification in low-energy lacustrine carbonates (Paleogene, Madrid Basin, Spain). Sedimentary Geology 151, 107–126.

Calvo, J.P., McKenzie, J., Vasconcelos, C., 2003. Microbially mediated lacustrine dolomite formation: evidence and current research trends. In: Valero-Garcés, B.L. (Ed.), Limnogeology in Spain: A Tribute to Kerry Kelts. Consejo Superior de Investigaciones Cientificas, Madrid, pp. 229–251.

Capuzzo, N., Wetzel, A., 2004. Facies and basin architecture of the Late Carboniferous Salvan-Dorénaz continental basin (Western Alps, Switzerland/France). Sedimentology 51, 675–697.

Çiftçi, B., Bozkurt, E., 2010. Structural evolution of the Gediz Graben, SW Turkey: temporal and spatial variation of the graben basin. Basin Research 22, 846–873.

Collins, A.S., Robertson, A.H.F., 1997. Lycian melange, southwestern Turkey: an emplaced Late Cretaceous accretionary complex. Geology 25, 255–258.

Collins, A.S., Robertson, A.H.F., 1998. Processes of Late Cretaceous to Late Miocene episodic thrust-sheet translations in the Lycian Taurides, SW Turkey. Journal of the Geological Society of London 155, 759–772.

Combourieu Nevout, N., Vergnaud Grazzini, C., 1991. Late Pliocene northern hemisphere glaciations: the continental and marine responses in the central Mediterranean. Quaternary Science Reviews 10, 319–334.

Coplen, T.B., Kendall, C., Hopple, J., 1983. Comparison of stable isotope reference samples. Nature 302, 236–238.

Cour, P., 1974. Nouvelles techniques de détection des flux et des retombées polliniques. Pollen et Spores 16, 103–142.

Deng, S., Dong, H., Lv, G., Jiang, H., Yu, B., Bishop, M.E., 2010. Microbial dolomite precipitation using sulfate reducing and halophilic bacteria: results from Qinghai Lake, Tibetan Plateau, NW China. Chemical Geology 278, 151–159.

Dunagan, S.P., Driese, S.G., 1999. Control of terrestrial stabilization of late Devonian palustrine carbonate deposition: catskill magnafacies, New York, USA. Journal of Sedimentary Research 69, 772–783.

Dunagan, S.P., Turner, C.E., 2004. Regional paleohydrologic and paleoclimatic settings of wetland/lacustrine depositional systems in the Morrison Formation (Upper Jurassic), Western Interior, USA. Sedimentary Geology 167, 269–296.

Elliott Jr., W.S., Suttner, L.J., Pratt, L.M., 2007. Tectonically induced climate and its control on the distribution of depositional systems in a continental foreland basin, Cloverly and Lakota Formations (Lower Cretaceous) of Wyoming, U.S.A. Sedimentary Geology 202, 730–753.

Freytet, P., Plaziat, J.C., 1982. Continental carbonate sedimentation and pedogenesis — Late Cretaceous and Early Tertiary of Southern France. Contrib. Sedimentol., 12 (213 pp.).

García del Cura, M.A., Calvo, J.P., Ordóñez, S., Jones, B.F., Cañaveras, J.C., 2001. Petrographic and geochemical evidence for the formation of primary, bacterially induced lacustrine dolomite: La Roda 'white earth' (Pliocene, central Spain). Sedimentology 48, 897–915.

Gierlowski-Kordesch, E.H., 1998. Carbonate deposition in an ephemeral siliciclastic alluvial plain: Jurassic Shutte Meadow Formation, Hartford Basin, Newark Supergroup, USA. Palaeogeography, Palaeoclimatology, Palaeoecology 140, 161–184.

Gierlowski-Kordesch, E., Rust, B.R., 1994. The Jurassic East Berlin Formation, Hartford Basin, Newark Supergroup (Connecticut and Massachusetts): a saline lake–playa–alluvial plain system. In: Renaut, R.W., Last, W.M. (Eds.), Sedimentology and Geochemistry of Modern and Ancient Saline Lakes: SEPM Special Publication, 50, pp. 249–265.

Goldsmith, J.R., Graf, D.L., 1958. Relations between lattice constraints and composition of the Ca–Mg carbonates. American Mineralogist 43, 84–101.

Goldsmith, J.R., Graf, D.L., Heard, H.C., 1961. Lattice constants of the calcium–magnesium carbonates. American Mineralogist 46, 453–457.

Gürer, Ö.M., Sarıca-Filoreau, N., Özburan, M., Sangu, E., Doğan, B., 2009. Progressive development of the Büyük Menderes Graben based on new data, western Turkey. Geological Magazine 146, 652–673.

Hadlari, T., Rainbird, R.H., Donaldson, J.A., 2006. Alluvial, eolian and lacustrine sedimentology of a Paleoproterozoic half-graben, Baker Lake Basin, Nunavut, Canada. Sedimentary Geology 190, 47–70.

Hardy, R.G., Tucker, M.E., 1988. X-ray powder diffraction of sediments. In: Tucker, M.E. (Ed.), Techniques in Sedimentology. Blackwell Science Publishers, Oxford, pp. 191–228.

Huerta, P., Armenteros, I., 2005. Calcrete and palustrine assemblages on a distal alluvial-floodplain: a response to local subsidence (Miocene of the Duero basin, Spain). Sedimentary Geology 177, 253–270.
Jiang, Z., Chen, D., Qiu, L., Liang, H., Ma, J., 2006. Source-controlled carbonates in a small Eocene half-graben lake basin (Shulu Sag) in central Hebei Province, North China. Sedimentology 54, 265–292.
Jiménez-Moreno, G., Rodríguez-Tovar, F.-J., Pardo-Igúzquiza, E., Fauquette, S., Suc, J.-P., Müller, P., 2005. High-resolution palynological analysis in late early–middle Miocene core from the Pannonian Basin, Hungary: climatic changes, astronomical forcing and eustatic fluctuations in the Central Paratethys. Palaeogeography, Palaeoclimatology, Palaeoecology 216, 73–97.
Jiménez-Moreno, G., Suc, J.-P., Fauquette, S., 2010. Miocene to Pliocene vegetation reconstruction and climate estimates in the Iberian Peninsula from pollen data. Review of Palaeobotany and Palynology 162, 403–415.
Jiménez-Moreno, G., Anderson, R.S., Atudorei, V., Toney, J.L., 2011. A high-resolution record of vegetation, climate, and fire regimes in the mixed conifer forest of northern Colorado (USA). Geological Society of America Bulletin 123, 240–254.
Joannin, S., Quillévéré, F., Suc, J.-P., Lécuyer, C., Martineau, F., 2007. Early Pleistocene climate changes in the central Mediterranean region as inferred from integrated pollen and planktonic foraminiferal stable isotope analyses. Quaternary Research 67, 264–274.
Kastelli, M., 1971. Denizli-Sarayköy-Çubukdağ-Karacasu alanının jeolojisi incelemesi. Mineral Res. Expl. Direct. Turkey (MTA), Scientific Report No: 4573, Ankara, Turkey (in Turkish, unpublished).
Kidder, D.L., Gierlowski-Kordesch, E.H., 2005. Impact of grassland radiation on the nonmarine silica cycle and Miocene diatomite. Palaios 20, 198–206.
Konak, N., Şenel, M., 2002. Geological map of Turkey in 1:500000 scale: Denizli sheet. Mineral Res. Expl. Direct. Turkey (MTA), Ankara, Turkey (in Turkish, unpublished).
Lee, S.H., Chough, S.K., 1999. Progressive changes in sedimentary facies and stratal patterns along the strike-slip margin, northeastern Jinan Basin (Cretaceous), southwest Korea: implications for differential subsidence. Sedimentary Geology 123, 81–102.
Machette, M.N., 1985. Calcic soils of the south western United States. In: Weide, D.L. (Ed.), Soils and Quaternary Geology of the Southwestern United States: Geol. Soc. Am. Spec. Pap., 203, pp. 1–21.
Makaske, B., 2001. Anastomosing rivers: a review of their classification, origin and sedimentary products. Earth-Science Reviews 53, 149–196.
Mayayo, M.J., Bauluz, B., López-Galindo, A., González-López, J.M., 1996. Mineralogy and geochemistry of the carbonates in the Catalayud Basin (Zaragoza, Spain). Chemical Geology 130, 123–136.
Meléndez, N., Liesa, C.L., Soria, A.R., Meléndez, A., 2009. Lacustrine system evolution during early rifting: El Castellar Formation (Galve sub-basin, Central Iberian Chain). Sedimentary Geology 222, 64–77.
Mercier, J.L., Sorel, D., Vergely, P., 1989. Extensional tectonic regimes in the Aegean basins during the Cenozoic. Basin Research 2, 49–71.
Meyers, P.A., Lallier-Vergès, E., 1999. Lacustrine sedimentary organic matter records of late Quaternary paleoclimates. Journal of Paleolimnology 21, 345–372.
Miall, A.D., 1996. The Geology of Fluvial Deposits.Springer-Verlag, Heidelberg (582 pp.).
Nebert, K., 1955. Bozdoğan ve Karacasu'daki genç Neojen körfezleri jeoloji raporu. Mineral Res. Expl. Direct. Turkey (MTA), Scientific Report No. 2511, Ankara, Turkey (in Turkish, unpublished).
Okay, A.İ., 1989. Denizli'nin güneyinde Menderes masifi ve Likya naplarının jeolojisi. Bulletın of the Mineral Research and Explorатıon Instıtute of Turkey (MTA) 109, 45–58.
Pamir, H.N., Erentöz, C., 1974. Geological maps of Turkey in 1:500.000 scale: Denizli sheet. General Directorate of the Mineral Research and Exploration of Turkey (MTA), Ankara.
Paz, J.D.S., Rossetti, D.F., 2006. Paleohydrology of an Upper Aptian lacustrine system from northeastern Brazil: integration of facies and isotopic geochemistry. Palaeogeography, Palaeoclimatology, Palaeoecology 241, 247–266.
Peryam, T.C., Dorsey, R.J., Bindeman, I., 2011. Plio-Pleistocene climate change and timing of Peninsular Ranges uplift in southern California: evidence from paleosols and stable isotopes in the Fish Creek–Vallecito basin. Palaeogeography, Palaeoclimatology, Palaeoecology 305, 65–74.
Popescu, S.-M., 2006. Late Miocene and Early Pliocene environments in the southwestern Black Sea region from high-resolution palynology of DSDP Site 380A (Leg 42B). Palaeogeography, Palaeoclimatology, Palaeoecology 238, 64–77.
Popescu, S.-M., Biltekin, D., Winter, H., Suc, J.-P., Melinte-Dobrinescu, M.C., Klotz, S., Rabineau, M., Combourieu-Nebout, N., Clauzon, G., Deaconu, F., 2010. Pliocene and Lower Pleistocene vegetation and climate changes at the European scale: long pollen records and climatostratigraphy. Quaternary International 1–2, 152–167.
Purvis, M., Robertson, A., 2005. Sedimentation of the Neogene–Recent Alaşehir (Gediz) continental graben system used to test alternative tectonic models for western (Aegean) Turkey. Sedimentary Geology 173, 373–408.
Quézel, P., Médail, F., 2003. Ecologie et biogéographie des forêts du basin méditerranéen.Elsevier, France (571 pp.).
Ramos, E., Cabrera, L., Hagemann, H.W., Pickel, W., Zamarreño, I., 2001. Paleogene lacustrine record in Mallorca (NW Mediterranean, Spain): depositional, palaeogeographic and palaeoclimatic implications for the ancient southeastern Iberian margin. Palaeogeography, Palaeoclimatology, Palaeoecology 172, 1–37.
Ridgway, K.D., DeCelles, P.G., 1993. Stream-dominated alluvial fan and lacustrine depositional systems in Cenozoic strike-slip basins, Denali fault system, Yukon Territory, Canada. Sedimentology 40, 645–666.
Ring, U., Johnson, C., Hetzel, R., Gessner, K., 2003. Tectonic denudation of a Late Cretaceous–Tertiary collisional belt regionally symmetric cooling patterns and their relation to extensional faults in the Anatolide belt of western Turkey. Geological Magazine 140, 1–21.
Roberts, S.C., 1988. Active normal faulting in central Greece and Western Turkey. Unpublished Ph.D. Thesis Cambridge Univ., United Kingdom.
Rust, B.R., Nanson, G.C., 1989. Bedload transport of mud as pedogenic aggregatesin modern ancient rivers. Sedimentology 36, 291–306.
Sáez, A., Cabrera, L., 2002. Sedimentological and palaeohydrological responses to tectonics and climate in a small, closed, lacustrine system: Oligocene As Pontes Basin (Spain). Sedimentology 49, 1073–1094.
Sáez, A., Inglès, M., Cabrera, L., de las Heras, A., 2003. Tectonic–palaeoenvironmental forcing of clay–mineral assemblages in nonmarine settings: the Oligocene–Miocene As Pontes Basin (Spain). Sedimentary Geology 159, 305–324.
Sáez, A., Anadón, P., Herrer, M.J., Moscariello, A., 2007. Variable style of transition between Paleogene fluvial fan and lacustrine systems, South Pyrenean Foreland, NE Spain. Sedimentology 54, 367–390.
Salvany, J.M., Muñoz, A., Pérez, A., 1994. Nonmarine evaporitic sedimentation and associated diagenetic processes of the southwestern margin of the Ebro basin (Lower Miocene), Spain. Journal of Sedimentary Research A64, 190–203.
Sánchez-Román, M., Vasconcelos, C., Schmid, T., Dittrich, M., McKenzie, J.A., Zenobi, R., Rivadeneyra, M.A., 2008. Aerobic microbial dolomite at the nanometer scale: implications for the geologic record. Geology 36, 879–882.
Sanz-Montero, M.E., Rodríguez-Aranda, J.P., García del Cura, M.A., 2008. Dolomite–silica stromatolites in Miocene lacustrine deposits from the Duero Basin, Spain: the role of organotemplates in the precipitation of dolomite. Sedimentology 55, 729–750.
Sanz-Montero, M.E., Rodríguez-Aranda, J.P., García del Cura, M.A., 2009. Bioinduced precipitation of barite and celestite in dolomite microbialites: examples from Miocene lacustrine sequences in the Madrid and Duero Basins, Spain. Sedimentary Geology 222, 138–148.
Şengör, A.M.C., 1987. Cross faults and differential stretching of hanging wails in regions of low angle normal faulting: examples from western Turkey. In: Coward, M.P., Dewey, J.F., Hancock, P.L. (Eds.), Continental Extensional Tectonics: Geol. Soc. London Spec. Publ., 28, pp. 575–589.
Şengör, A.M.C., Görür, N., Şaroğlu, F., 1985. Strike-slip faulting and related basin formation in zones of tectonic escape: Turkey as a case study. In: Biddle, K.D., Christie-Blick, N. (Eds.), Strike-slip Deformation, Basin Formation and Sedimentation: SEPM Spec. Publ., 17, pp. 227–264.
Sharp, Z.D., Durakiewicz, T., Migaszewski, Z.M., Atudorei, V.N., 2002. Anti phase hydrogen and oxygen isotope periodicity in chert nodules. Geochimica et Cosmochimica Acta 66, 2865–2873.
Smittenberg, R.H., Baas, M., Schouten, S., Sinninghe Damsté, J.S., 2005. The demise of the algae *Botryococcus braunii* from a Norwegian fjord was due to early eutrophication. The Holocene 15, 133–140.
Sun, S., 1990. Denizli-Uşak Arasının Jeolojisi ve Linyit Olanakları. Mineral Res. Expl. Direct. Turkey (MTA), Scientific Report No: 9985, Ankara, Turkey (in Turkish, unpublished).
Talbot, M.R., 1990. A review of the palaeohydrological interpretation of carbon and oxygen isotopic ratios in primary lacustrine carbonates. Chemical Geology 80, 261–279.
Talbot, M.R., Kelts, K., 1990. Paleolimnological signatures from carbon and oxygen isotopic ratios in organic carbon rich lacustrine sediments. In: Katz, B.J. (Ed.), Lacustrine Basin Exploration — Case Studies and Modern Analogs: AAPG Mem., 50, pp. 99–112.
Temel, A., Gündoğdu, M.N., 1996. Zeolite occurrences and erionite–mesothelioma relationship in Cappadocia region, Central Anatolia, Turkey. Mineralium Deposita 31, 539–547.
Ten Veen, J.H., Boulton, S.J., Alçiçek, M.C., 2009. From palaeotectonics to neotectonics in the Neotethys realm: the importance of kinematic decoupling and inherited structural grain in SW Anatolia (Turkey). Tectonophysics 473, 261–281.
Utrilla, R., Vázquez, A., Anadón, P., 1998. Paleohydrology of the Upper Miocene Bicorb Lake (eastern Spain) as inferred from Stable isotopic data from inorganic carbonates. Sedimentary Geology 121, 191–206.
Valero-Garcés, B.L., Kelts, K., 1995. A sedimentary facies model for perennial and meromictic saline lakes: Holocene Medicine Lake Basin, South Dakota, USA. Journal of Sedimentary Research 14, 123–149.
van Hinsbergen, D.J.J., 2010. A key extensional metamorphic complex reviewed and restored: the Menderes Massif of western Turkey. Earth-Science Reviews 102, 60–76.
van Hinsbergen, D.J.J., Schmid, S.M., 2012. Map-view restoration of Aegean–west Anatolian accretion and extension since the Eocene. Tectonics 31, 1–40.
Verrecchia, E.P., 2007. Lacustrine and palustrine geochemical sediments. In: Nash, D.J., McLaren, S.J. (Eds.), Geochemical Sediments and Landscapes. Blackwell Publishing, Oxford, pp. 298–329.